PALACKÝ UNIVERSITY OLOMOUC
FACULTY OF SCIENCE
DEPARTMENT OF EXPERIMENTAL PHYSICS

Master's Thesis

Piezoelectric energy harvesters based on microstructured polymer layers

VOJTĚCH SKOUMAL

PALACKÝ UNIVERSITY OLOMOUC
FACULTY OF SCIENCE
DEPARTMENT OF EXPERIMENTAL PHYSICS

Master's Thesis

Piezoelectric energy harvesters based on microstructured polymer layers

Author:	**Bc. Vojtěch Skoumal**
Study programme:	N1701 Physics
Field of study:	3942T001 Nanotechnology
Form of study:	Full-time
Supervisor:	doc. RNDr. Jiří Pechoušek Ph.D.
Thesis submitted on:	May 12, 2023

UNIVERZITA PALACKÉHO V OLOMOUCI

PŘÍRODOVĚDECKÁ FAKULTA

KATEDRA EXPERIMENTÁLNÍ FYZIKY

Diplomová práce

Piezoelektrické generátory z mikrostrukturovaných polymerních vrstev

Vypracoval:	**Bc. Vojtěch Skoumal**
Studijní program:	N1701 Fyzika
Studijní obor:	3942T001 Nanotechnologie
Forma studia:	Prezenční
Vedoucí diplomové práce:	doc. RNDr. Jiří Pechoušek Ph.D.
Termín odevzdání práce:	12. května 2023

Declaration

I hereby declare that I have written this Master's Thesis and performed all the presented research and experimental tasks by myself, while being supervised by doc. RNDr. Jiří Pechoušek Ph.D. I also state that every resource used is properly cited.

In Olomouc on May 12, 2023

....

Bc. Vojtěch Skoumal

Acknowledgments

VOJTĚCH SKOUMAL

Bibliographical identification

Autor's first name and surname	Bc. Vojtěch Skoumal
Title	Piezoelectric energy harvesters based on microstructured polymer layers
Type of thesis	Master
Department	Department of Experimental Physics
Supervisor	doc. RNDr. Jiří Pechoušek Ph.D.
The year of presentation	2023
Abstract	Flexible piezoelectric generators are currently receiving a great deal of interest thanks to their great application potential in power generation, biomedicine, or monitoring of buildings and machines. This master thesis focuses on the manufacturing of such flexible piezoelectric generators based on polyvinylidene difluoride films prepared by electrospinning, casting, and water-assisted curing. The goal of this work is to design and construct experimental apparatus for said methods, manufacture generators based on polymer layers, evaluate their performance, and compare the methods of synthesis.
Keywords	electrospinning, PVDF, energy harvesting
Number of pages	56
Number of appendices	0
Language	english

Bibliografická identifikace

Jméno a příjmení autora	Bc. Vojtěch Skoumal
Název práce	Piezoelektrické generátory z mikrostrukturovaných polymerních vrstev
Typ práce	Diplomová
Pracoviště	Katedra experimentální fyziky
Vedoucí práce	doc. RNDr. Jiří Pechoušek Ph.D.
Rok obhajoby práce	2023
Abstrakt	Flexibilní piezoelektrické generátory se v současné době těší velkému zájmu díky svému velkému aplikačnímu potenciálu v oblasti výroby energie, biomedicíny nebo monitorování budov a strojů. Tato diplomová práce se zaměřuje na výrobu takových flexibilních piezoelektrických generátorů na bázi polyvinyliden difluoridových vrstev připravených elektrostatickým zvlákňováním, litím a vytvrzováním za pomoci vody. Cílem této práce je navrhnout a zkonstruovat experimentální aparaturu pro uvedené metody, vyrobit generátory na bázi polymerních vrstev, vyhodnotit jejich výkon a porovnat metody syntézy.
Klíčová slova	elektrostatické zvlákňování, PVDF, získávání energie
Počet stran	56
Počet příloh	0
Jazyk	anglický

Contents

Introduction

Flexible piezoelectric generators are currently receiving a great deal of interest thanks to their great application potential in power generation, biomedicine, or monitoring of buildings and machines. The desired flexibility is achieved by replacing brittle ceramics with polymers. This master thesis focuses on the manufacturing of such flexible piezoelectric generators based on polyvinylidene difluoride films prepared by three methods. The goal of this work is to design and construct experimental apparatus for said methods and prepare polymer films. Then electro-mechanical measurements will be designed and performed on generators based on polymer layers in order to evaluate their performance and compare the methods of synthesis.

Chapter 1

Theoretical background

The subject of this thesis is piezoelectric energy harvesters based on microstructured polymer layers. Therefore in the following sections, the piezoelectric effect is introduced as well as polymers and energy harvesting itself.

1.1 Polymers

A polymer is a large chain-like molecule (macromolecule) built up by the repetition of small chemical units. This unit is also called *structural unit* and it is a residue of a single *monomer* after the process of polymerization[1] [1]. The monomer must have either reactive functional groups, such as amino groups ($-NH_2$), or double bonds that can react under appropriate conditions to form a covalent bond between the repeating units. Such strong bonds form the backbone of the polymer chain. [2]

Polymers in the solid state may be amorphous or crystalline. But the most common state is a combination of both at the same time. This is called *semicrystalline* state and is described by a *degree of crystallinity*[2]. The highest degree of crystallinity is typically achieved by slow evaporation of a polymer solution or slow cooling from a molten state. [1]

One of the most important parameters of a polymer is *molecular weight.* The molecular weight of a polymer is the sum of the atomic weights of the individual atoms that make up the molecule [3]. It indicates the average length of the polymer chains of a bulk material. Polymer chain lengths have a certain distribution around this mean value and the shape of this distribution depends on the method of synthesis and the mean chain length itself. Even though molecular weight is a microscopic property, it has a strong influence on the macroscopic behavior of the material. For example, low molecular weight polymerization products such as *dimers*, *trimers*, *tetramers*, etc. (often referred to as *oligomers*) generally have undesirable thermal and mechanical properties. A high degree of polymerization is usually required for a material to acquire useful properties and be suitably described as a polymer. [1]

---

[1]Process by which relatively small molecules, called monomers, combine chemically to form a very large chain or network of molecules, called a polymer.

[2]a fraction of a polymer bulk in crystalline state

1.2 Piezoelectricity

Piezoelectricity is the ability of certain solid materials to generate electric potential difference when subjected to mechanical stress along a polar axis. The piezoelectric effect can be observed in those materials, which possess a polar axis without a center of symmetry. The *direct* piezoelectric effect occurs when a stress is applied, causing charge centers to shift and creating a dipole as shown in Figure 1.1. The intensity and direction of charge transfer depend on the direction and magnitude of compression. An indirect or *converse* piezoelectric effect is defined as the generation of a mechanical displacement by applying opposite electric potentials to two opposite sites of a material. [4]
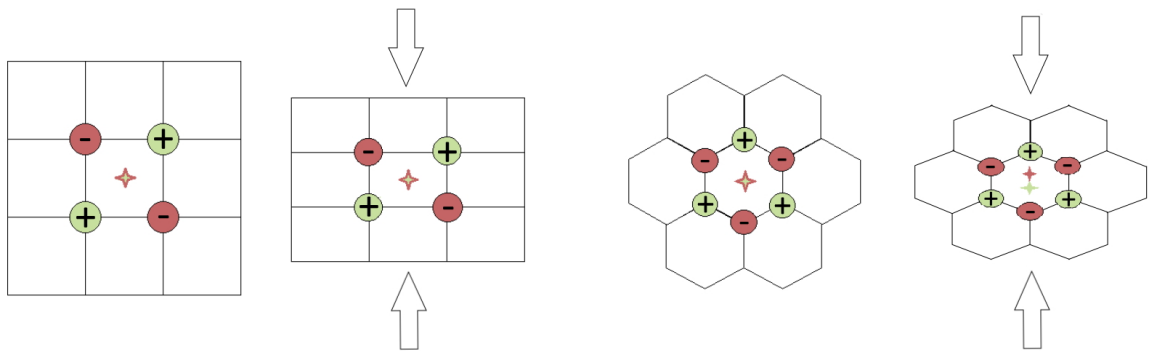

Figure 1.1: External force acting on an ionic crystal with (left) and without (right) inversion symmetry, adapted from [5]

One of the most important parameters of a piezoelectric element is its *resonant* (and anti-resonant) *frequency.* The resonant frequency is a frequency at which the piezoelectric element transfers energy between mechanical and electrical form the most efficiently. On the other hand, anti-resonant frequency is the right opposite – the least efficient frequency. In order to determine the resonant frequency of a piezoelectric element one can simply electrically stimulate the element at different frequencies and look for the biggest displacement amplitude. A more sophisticated way includes measuring the frequency dependency of the element's impedance (typically with an impedance analyzer). In Figure 1.2 said dependency is shown for both piezoelectric and dielectric elements. For the piezoelectric element, two significant points can be found. The resonance frequency can be determined from the local minimum of the impedance function and similarly, the anti-resonant frequency can be determined from the local maximum of the impedance function. For one piezoelectric element, multiple resonant frequencies can be found. The number and the frequencies themselves depend on spatial vibration modes and piezoelectric constants of said element. But this is beyond the scope of this work. [6]

1.2.1 Piezoelectricity in ceramics

The piezoelectric effect is found in both natural and synthetic materials. Quartz is a natural example, while ferroelectric ceramics like $Pb(Zr_xTi_{1-x})O_3$ (PZT) are synthetic materials. Quartz has a weak but stable, and linear piezoelectric response, while PZT has a much stronger[3] but not so well-behaved response. [8]

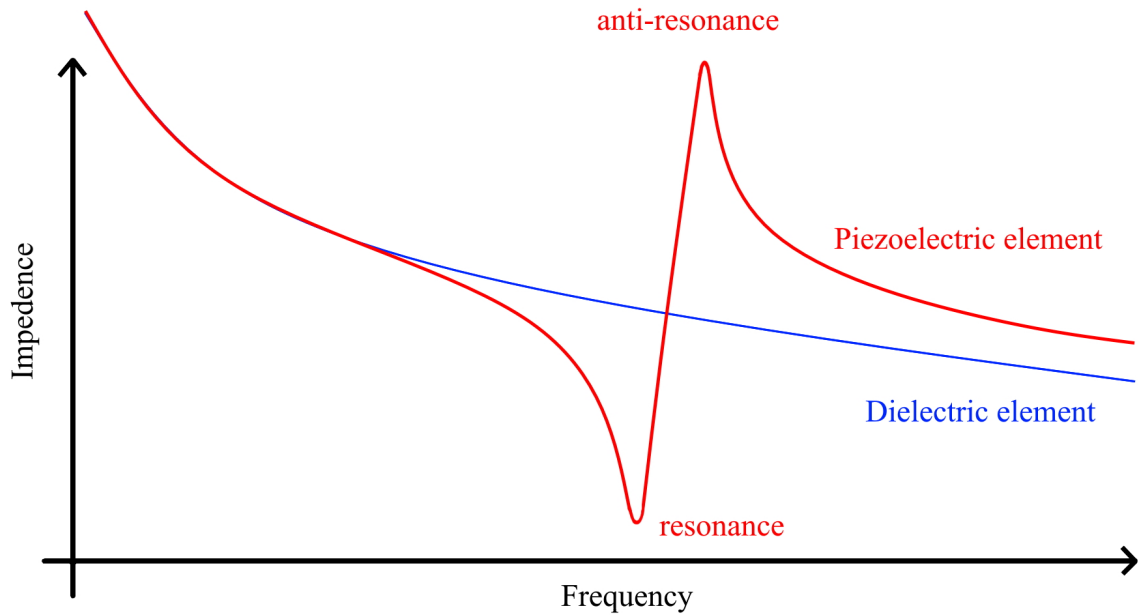[3]about two orders of magnitude higher than quartz

Figure 1.2: Frequency dependency of impedance for piezoelectric and dielectric element, inspired by [7]

The poling process involves applying a high DC electric field for a certain amount of time while heating the ceramic element in a dielectric oil bath. The electric field is usually in the order of kilovolts per millimeter of element thickness. The elevated temperature provides enough kinetic energy needed for the individual crystalline domains to align with the electric field. [9]

Piezoelectric applications can be divided into three categories: sensors, actuators, and high-frequency transducers. Piezoelectric sensors measure force, acceleration, and vibration through the direct effect. Actuators generate force and displacement using the converse effect, typically on a nanoscale. This is useful for precise displacement control, but alternative methods are needed for larger displacement applications, such as fuel injection actuators that require movement on a millimeter scale or higher. [8]

The biggest disadvantages of ceramic piezoelectric elements are often the strongly non-linear response, low biocompatibility, and a fundamental lack of the ability to perform static measurements. Also, ceramics are extremely brittle materials. This is limiting for a plethora of applications (e.g. bio-sensors and energy harvesting).

1.2.2 Piezoelectricity in polymers

The most common form of piezoelectric polymers is semicrystalline polymers. The morphology of such polymers consists of crystallites dispersed within amorphous regions. Most semicrystalline polymers have several polymorphic phases, some of which may be polar. Similarly to ceramic elements, the polling process can be used here to enhance the piezoelectric effect. An electric field of dozens of kilovolts per millimeter of element thickness is typically sufficient to affect crystalline orientation. [10, 11]

The biggest advantage of polymer piezoelectrics over ceramics is their flexibility. This, together with their low reactivity, makes them a perfect candidate for biocompatible piezoelectric applications. Polymers are also lightweight compared to ceramics and exhibit lower acoustic and mechanical impedance. [10]

The price for all those advantages is a significant decrease in piezoelectric response. Polymer piezoelectric constants are often several orders of magnitude smaller than those of ceramics.

1.3 Polyvinylidene difluoride

Polyvinylidene difluoride or PVDF is a highly inert thermoplastic fluoropolymer produced by the polymerization of vinylidene difluoride. The structural formula of both PVDF and vinylidene difluoride are shown in Figure 1.3. Based on the structure of the PVDF chain, we distinguish 3 phases: α, β, and γ. Structure schematics of all phases are shown in Figure 1.4. The α phase is the most thermodynamically stable. It is commonly used as a surface treatment for materials due to its low thermal conductivity and high chemical and thermal resistance. The β phase exhibits the best piezoelectric properties. Due to its high chemical resistance and biocompatibility, it is used in many sensors, actuators, and generators – energy harvesting systems.
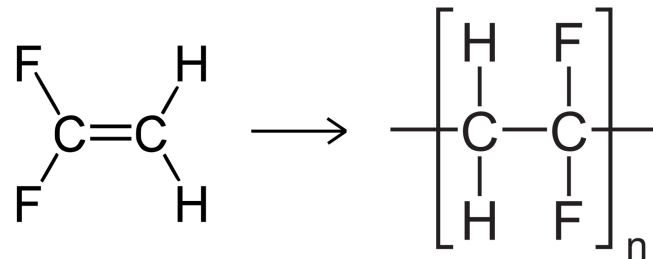

Figure 1.3: Polymerization of vinylidene difluoride leading to the formation of PVDF
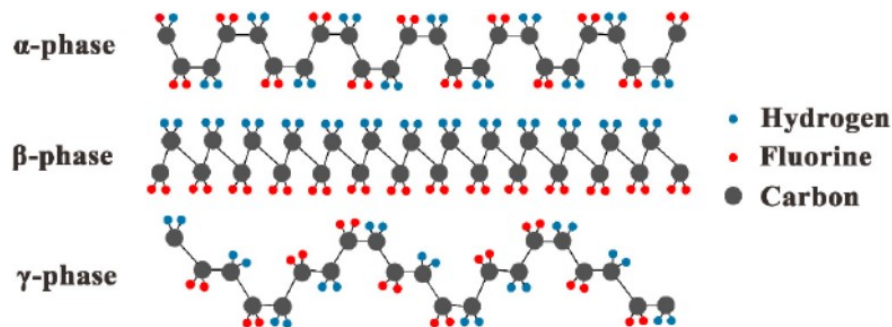
Figure 1.4: Structures of α, β and γ phase PVDF, adapted from [12]

1.4 Electrospinning

Electrospinning is a technique for the fabrication of long polymer fibers in micron and submicron range from solution. The experimental apparatus consists of three key parts: high voltage power source, syringe pump, and collector. The power source should be able to provide dozens of kilovolts of DC voltage. The syringe pump serves as a source of material and its typical output is in milliliters per hour. The collector is a flat conductive target for the deposition of fibers. This method takes advantage of a strong electric field forming a *Taylor cone* from a solution surface. After the cone

emerges material is further transported towards the collector in a form of a thick fiber which is continuously thinned by electrostatic force. A schematic of the electrospinning apparatus is shown in Figure 1.5.
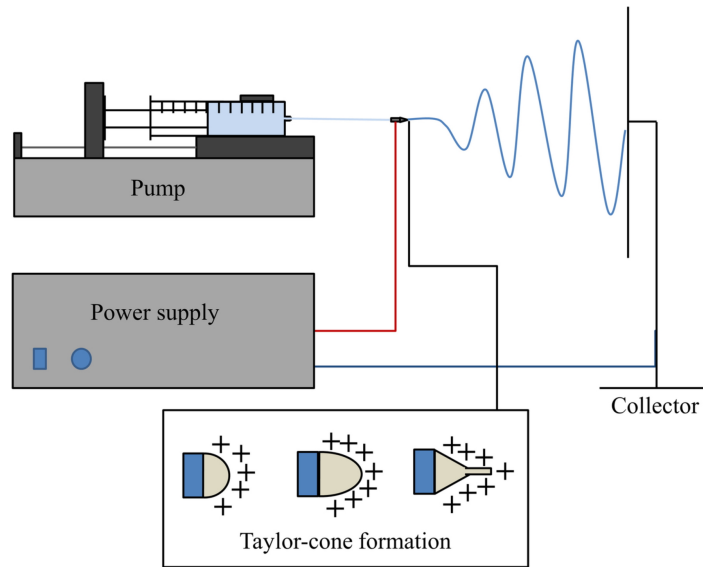

Figure 1.5: Schematic of electrospinning apparatus and Taylor cone formation mechanics, adapted from [13]

Requirements for successful electrospinning according to [2]:

- solubility of the desired polymer,

- low vapor pressure of the solvent,

- suitable viscosity and surface tension of the solution,

- electric field adequate to overcome the viscosity and surface tension of the polymer solution.

1.4.1   Preparation of oriented fibers

So far electrospinning of unoriented fibers was discussed. In order to prepare fibers with a dominant orientation rotating collector has to be introduced. When a fiber is deposited on a moving surface its orientation is influenced. To gain a strong dominant orientation fiber speed towards the collector must be negligible compared to the surface speed. A schematic of an experimental setup for the preparation of oriented fibers is shown in Figure 1.6.

The rotating collector is usually a cylinder or a disc. It can be made of solid steel or just a wire mesh. Conductivity and ability to withstand the centrifugal force caused by high rpm are required.

The ability to prepare oriented fibers has a potential to enhance the piezoelectric effect of a prepared element [14]. Other potential applications of oriented fibers are air or other gas filters [15], seawater desalination filters [16] or artificial tissue [17].
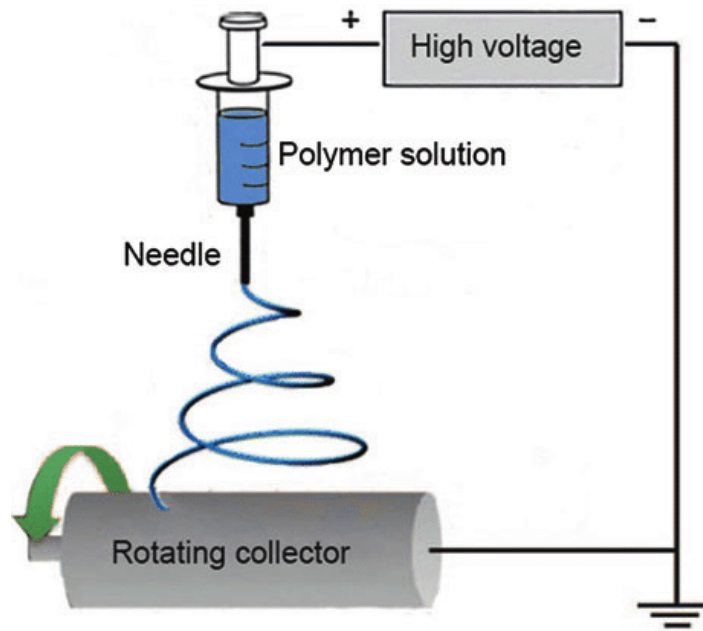
Figure 1.6: Schematic of an experimental setup for preparation of oriented fibers, adapted from [18]

1.5 Energy harvesting

Energy harvesting could be defined as a process of extraction of small amounts of energy from the environment. In this work, only energy harvesting of mechanical vibrations will be discussed but gaining energy from radio waves, temperature differences or light can be called energy harvesting as well. A typical use case is powering small standalone sensors where conventional sources of energy like batteries cannot be used[4] [19, 20].

The piezoelectric energy harvesting apparatus consists of three important parts. The first part is a piezoelectric element, for example, a thin PZT cantilever with two electrodes and a weight on the tip to enhance the displacement amplitude and also tune the resonant frequency. Next is a current rectifier because the piezoelectric response resembles alternating current[5]. The last part is energy storage – capacitor or battery. This basic setup powering a LED diode is shown in Figure 1.7 together with the shape of the electric signal in each step. In order to optimize the efficiency of this setup more complicated circuit can be introduced using a commercially available energy harvesting integrated circuit LTC3588. [21]

---

[4]Typically when the sensor is hard (expensive) to reach, for example, Carlson strain meter embedded in a bridge structure.

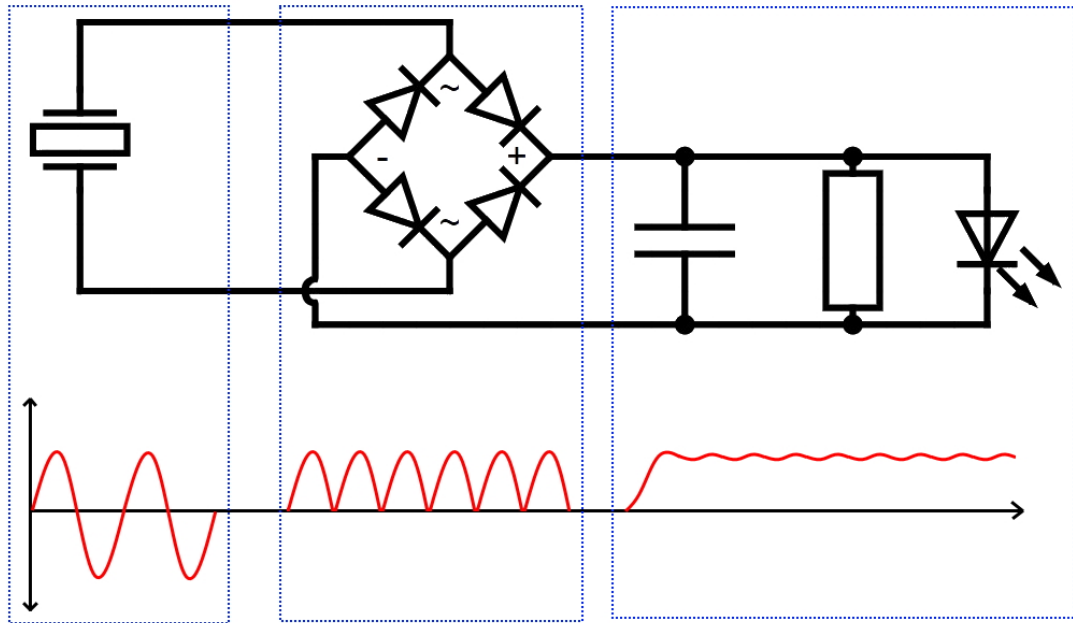[5]It is both positive and negative in one cycle.

Figure 1.7: Basic energy harvesting circuit and typical waveforms in respective areas of the circuit

Piezoelectric elements for energy harvesting systems (generators) based on PVDF films are the subject of many studies. Their typical performance in terms of generated peak-to-peak voltage range from tens or hundreds of millivolts [22, 23] to a few volts [24, 25]. In the literature, electrospun PVDF generators occur the most often. Other interesting methods including electrohydrodynamic pulling and template-assisted growing are described in [26] but they are beyond the scope of this work. As it was earlier demonstrated [27], PVDF generators are capable of charging a capacitor in an energy harvesting setup. Interesting proof of concept applications were performed as well. For example, PVDF generators were used for harvesting human exhaled air energy with a potential for monitoring applications [28]. The electrospun films were also used for manufacturing flexible wearable generators harvesting energy from human walk [25]. From the electrical response of this generator, researchers were even able to monitor different walking phases. Thus making a sensor with comparable performance to a gyroscope.

Chapter 2

Experimental part

So far the theoretical part was discussed. In this chapter, all the methods, devices, and materials used are introduced and explained. The aim of this master thesis is to create PVDF films using multiple methods and fabricate energy generators based on said films. In total three methods were used for film preparation, namely electrospinning, casting, and water-assisted fast curing. All of them start with a solution of PVDF and lead to either self-supported or substrate-supported films. Generators based on these layers were then tested for suitability for piezoelectric applications.

2.1   Chemicals and devices

Polyvinylidene difluoride used for all synthesis was kindly provided by Arkema company in powdered form as a free sample. Their prompt action should be considered a significant contribution to this work. Both acetone and dimethylformamide (DMF) were purchased from Lach-Ner company and are of an analytical grade.

 The thickness of polymer layers was measured by digital micrometer SOMETCZ DIN 863 T1. For impedance analysis impedance analyzer HIOKI IM 3570 was used. Desired amounts of chemicals were weighed by KERN ABJ-NM/ABS-N analytical scale. Magnetic stirring hotplate Heidolph MR Hei-Standard played a crucial role in the solution preparation process. Thanks to the author's internship in Thermo Fisher Scientific company prepared samples were characterized using a scanning electron microscope Axia ChemiSEM.

2.2   PVDF solution

Arkema company provided PVDF in a fine powdered form. All three methods used in this work require PVDF dissolved in a solution. In order to prepare such a solution DMF was chosen to be the main solvent. For all methods DMF was used as cosolvent together with acetone in a ratio 7:3 (DMF:acetone). The ratio was inspired by work [29] of a Turkish research team. Several solutions with different concentrations were prepared. All concentrations used in this work are weight over volume percentage ratios (w/V %). PVDF powder weight on an analytical scale was put together with the corresponding amount of DMF and acetone into a glass beaker. Desired amounts of both liquids were measured using a 5 ml syringe. The mixture was then heated to 50 °C and magnetically stirred at 100 rpm. This temperature rise caused rapid evaporation of solvents that could cause unwanted changes in concentration. This problem was

solved by a glass lid sealed by an embedded parafilm sheet. After one hour of stirring well homogenized solution formed.

The solutions thus formed were kept in PP chemical bottles before use. Typical storage time was under one week. Four samples were kept untouched in the dark for 3 months. Already after one month, visible changes appeared namely color change and viscosity rise. A photo of these four samples after three months is shown in Figure 2.1a (note that fresh solution is completely transparent). Higher concentrations undergo bigger changes. Samples with concentrations 15 % and 20 % hardened into a jelly-like form as shown in Figure 2.1b. This ascertainment led to shortening storage time as little as possible (mostly only a few hours).
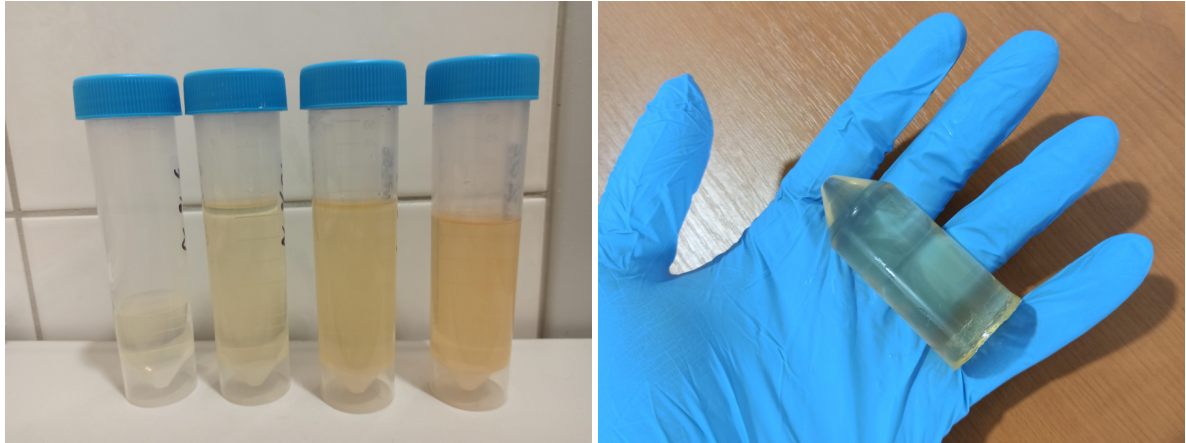
(a) Concentrations 5, 10, 15 and 20 %   (b) Concentration 20 %

Figure 2.1: Four solutions with different concentrations after three months

2.3   Electrospinning of PVDF

Electrospinning was chosen as one of the most promising methods for the preparation of PVDF films with interesting properties. Since this method has no history in our department whatsoever, the whole apparatus required by this method had to be designed, assembled, and tested. The following sections are intended to familiarize the reader with this apparatus. This includes an HV power source, a syringe pump, and two variations for the preparation of oriented and unoriented fibers.

2.3.1   High voltage power source

In the case of electrospinning HV power source plays a crucial role, since it is what makes the actual matter transport and shape forming happen. For our purposes, a 10 kV Phywe power supply was used. A commercial image of this device is shown in Figure 2.2. Its upper limit of 10 kV was binding but there is no other power source with better capabilities available at our department. This HV power source was used for curing cast polymer layers in an electric field as well. Details about this method are discussed in chapter 2.4.

Figure 2.2: Phywe 10 kV power supply

2.3.2 Syringe Pump

Although there are many commercially available syringe pumps, a cheaper solution was found for our purposes. All samples were prepared using a 3D printed pump shown in Figure 2.3. White parts we designed using online freeware 3D modeling tool and 3D printed from PLA on Prusa i3 MK3 printer. The model is available online on the author's GitHub [30]. Motion is controlled by a stepper motor 28BYJ-48 and an Arduino Uno. The remaining parts were obtained from a local hardware store. The pump is designed for 5 ml syringes. Flow rate range is from theoretically zero to 53 ml·h^{-1} (for more information about this topic see the following chapter). For all experiments, 0.5 mm Agani needles from Terumo company were used[1].
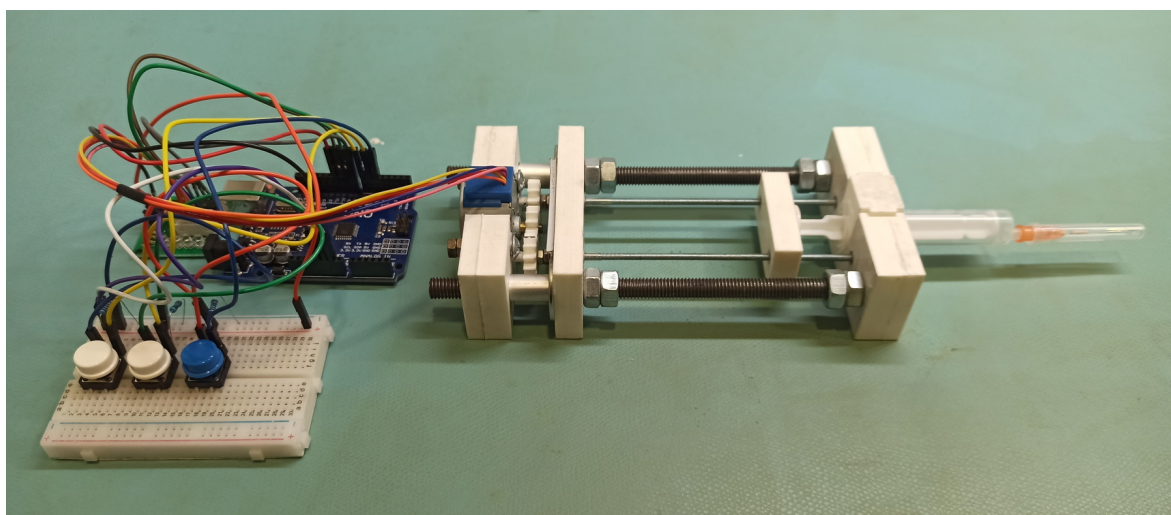

Figure 2.3: 3D printed syringe pump controlled by Arduino Uno board

---

[1]Syringes with bigger diameters were purchased as well, although only the 0.5 mm ones were used. The difference in needle diameter is expected to have no significant effect on the resulting fibers.

Controlling the pump

As mentioned above the pump is controlled by Arduino Uno board and ULN2003 driver. The source code for the pump is available on the author's GitHub [30] together with the 3D model. Users can control the pump motion using three buttons - two for both directions in full speed used during (un)loading and one for activating desired flow rate speed. Flow rate is determined by the time between steps of the stepper motor Δ. Knowing the syringe radius $r = 6.17$ mm, the screw thread pitch $p = 0.5$ mm and number of steps per rotation $N = 4096$ simple formula for flow rate Q can be derived

$$Q = \frac{\pi r^2 p}{N\Delta}. \tag{2.1}$$

For flow rate Q in ml·h⁻¹ and dwell time Δ in milliseconds we get

$$Q\left[\frac{\mathrm{ml}}{\mathrm{h}}\right] \approx \frac{52.557}{\Delta[\mathrm{ms}]}. \tag{2.2}$$

The smallest possible dwell time $\Delta = 1$ ms determines the maximal flow rate to be $Q \approx 52.6$ ml·h⁻¹. The minimal flow rate is on the other hand not so obvious since dwell time Δ can be theoretically infinite. The practical limitation is the continuity of the flow. Although the whole injection system has a reasonable rigidity, dwell times Δ above 1000 ms are not recommended. The whole pumping system was designed in such a way that our desired flow rates are safely in this available range. The only disadvantage of this syringe pump is the need for a computer for flow rate (dwell time) change. Hardware for a better solution, including LCD display for not only changing dwell time but also live display of information about volume injected and time elapsed, is already prepared but has not been yet implemented.

2.3.3 Unoriented fibers synthesis

A stationary target is used for collecting unoriented fibers. As a conductive layer aluminum foil or mylar was used. The collector's structure itself was made out of folded cardboard. One of the collectors used is shown in Figure 2.4a. The resulting apparatus for electrospinning unoriented fibers is shown in Figure 2.4b.
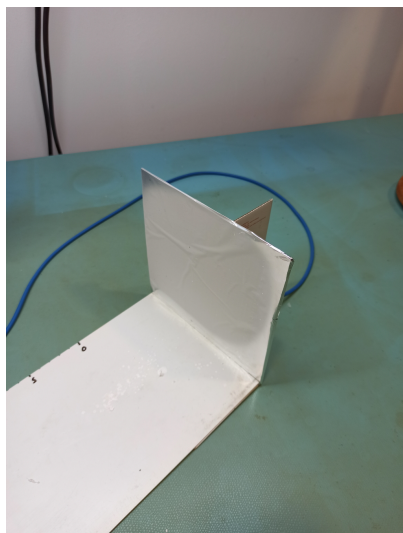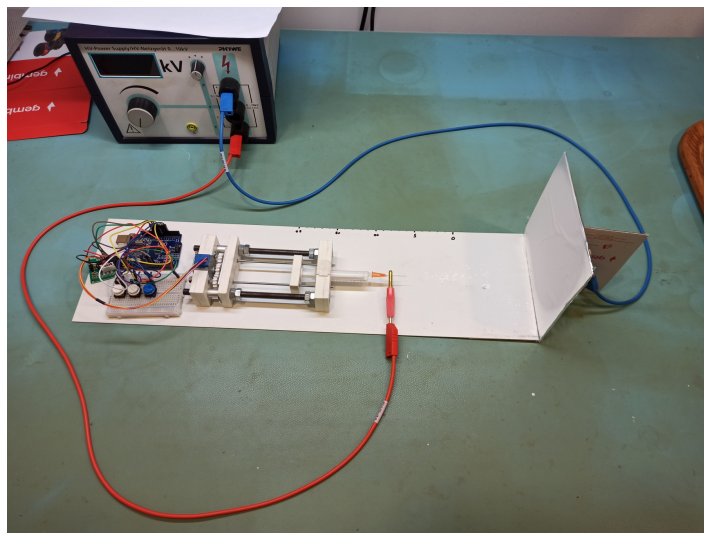
(a) Static collector (b) Apparatus for electrospinning unoriented fibers

Figure 2.4: Unoriented fibers synthesis

2.3.4 Oriented fibers synthesis

Unlike the unoriented fibers mentioned in the previous chapter, oriented fibers require a rotating collector. For this purpose specifically designed mounting stage with two exchangeable rotating cylinders of different diameters was assembled. The resulting apparatus for electrospinning oriented fibers is shown in Figure 2.5. Details about the rotor design are discussed in the following section.
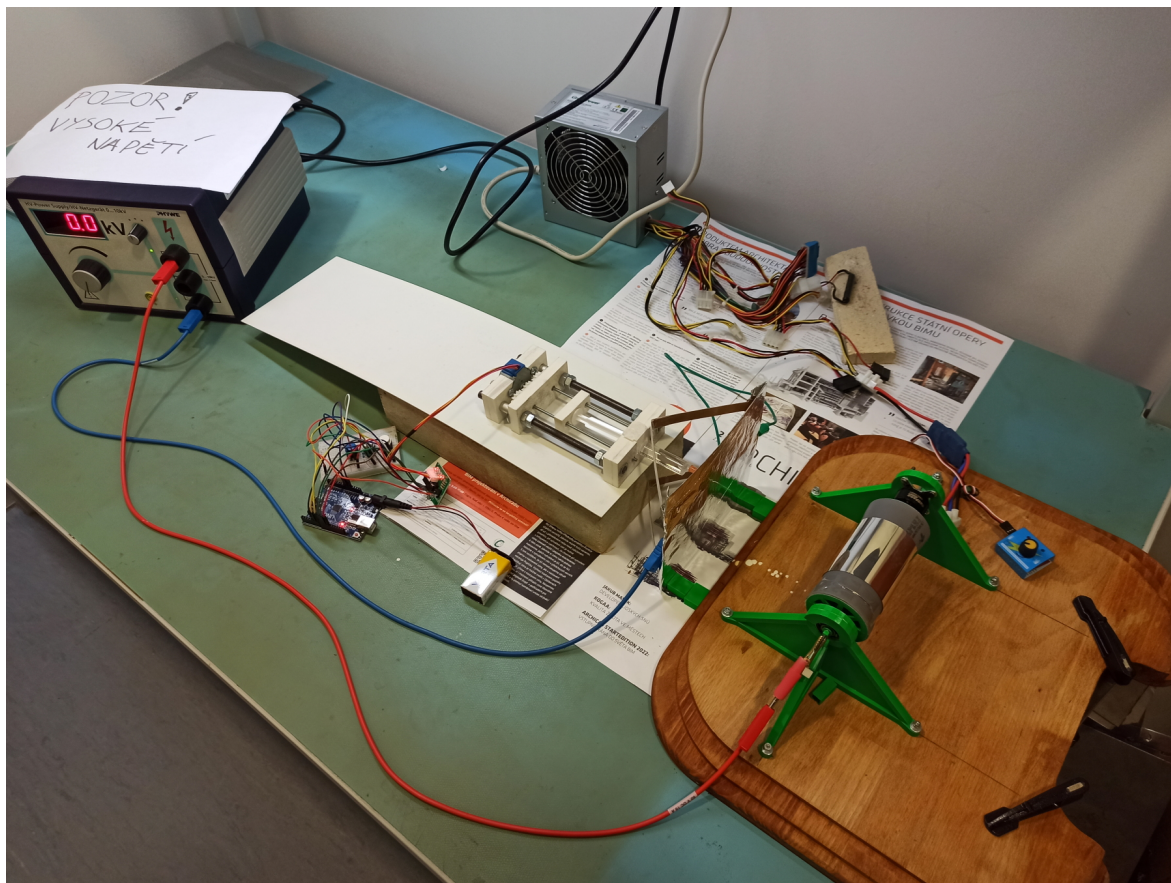

Figure 2.5: Experimental apparatus for oriented electrospun fibers preparation

Rotor design

Similarly to the syringe pump design, the rotor consists of 3D printed parts and an electric motor. 3D printed parts are made of PLA. The model is available on the author's GitHub [30] and a simple snapshot of said model is shown in Figure 2.6a. The rotary motion is provided by an electric motor SURPASS HOBBY C2826 powered by computer power source GreenPower AX350-60APN with FlyColor ESC regulator. The rotor rpm are controlled by a servo tester (potentiometer setting). All samples prepared by this method were created at maximum rpm. The electric motor rotates at 1000 rpm per volt. Since the used power source gives 12 V maximum rpm of this setup is 12 000 rpm.

This claim was experimentally tested with the help of a combination of a phototransistor and an infrared LED. This combination works as a reflective optical sensor. Because the sensor operates in the infrared spectrum, it does not interfere with ambient daylight. The signal output is higher when the sensor is pointing at a reflective[2]

---

[2]reflective in infrared spectrum

surface. Such surface was taped on the cylinder. When run at full speed periodic signal was observed on an oscilloscope with a frequency of 212 Hz (= 12 720 rpm) which confirmed the previous calculations. All samples were electrospun on a smaller rotor with diameter $r = 5$ cm. The pheriferal velocity is $v_p = 2\pi r f \approx 33.3$ m·s⁻¹.

Smooth rotation is ensured by a ball bearing from a local hardware store. The rotating cylinder is a combination of PVC pipe and 3D printed parts. The whole device is screwed to a wooden base which is attached to the table with metal clamps. In Figure 2.6 comparison of the rotor 3D model and the real device is shown.

This setup consists of three separate electrical circuits – the pump electronics, the rotor electronics, and the HV power supply. These circuits must remain insulated in order to avoid any malfunction or damage to the setup itself. The biggest technological challenge was to ensure a conductive connection between rotating and stationary parts while avoiding electrical discharge through the electric motor. Several unsuccessful attempts involving analogy to electric brushes positioned in the rotor's axis of rotation were tested. The final solution took advantage of the ball bearing conductivity. This way high voltage is conducted to the center of the cylinder and then by a flattened copper wire to the cylinder surface. Desired conductive substrate is then connected to this wire by copper tape. This method is applicable to both mylar and aluminum foil. But in Figure 2.5 old brush-like setup is shown with mylar as substrate, and the final setup is shown in Figure 2.6b. Finally, only the fact, that the whole rotating cylinder is made of insulators and an air gap is what prevents electrical discharge through the motor circuit.
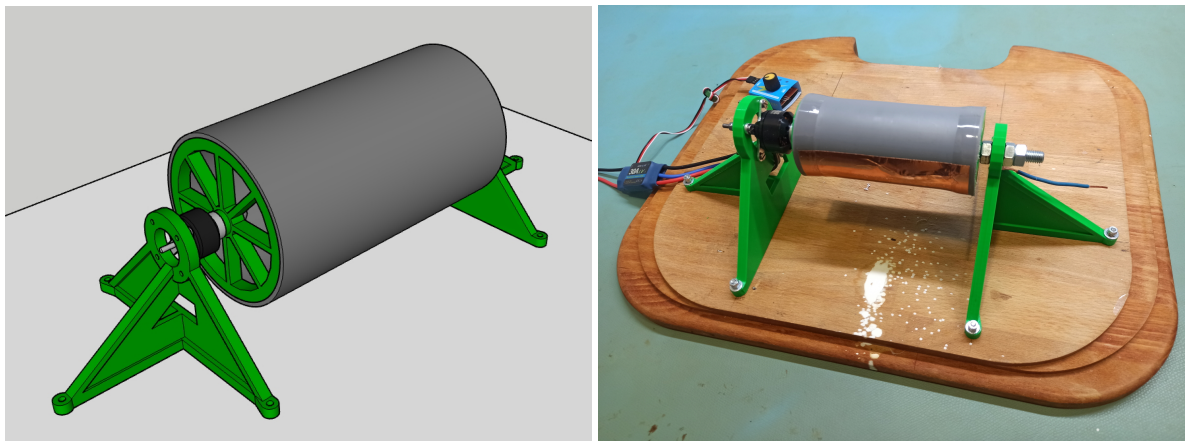
(a) 3D model of the rotor with 10 cm cylinder   (b) The real rotor with 5 cm cylinder

Figure 2.6: Comparison of the rotor 3D model and real device

2.4 Casting of PVDF

The simplest way to prepare PVDF film is to pour its solution onto a desired substrate. Unfortunately, even such an easy method has its problems and has to be tuned first.

In order to produce self-supported PVDF films glass (Petri dish) was used as substrate. Various amounts of solutions with four different concentrations ($c = 5$ %, 10 %, 15 % and 20 %) were tried. Some of the unsuccessful attempts are shown in Figure 2.7a. Here the two main problems are obvious. If the combination of concentration and quantity is not right, the drying solution either cracks or crumples. The best concentration turned out to be $c = 20$ %. Poring a solution of this concentration on

a substrate and then spreading it by a circular motion and just gravity force resulted in a transparent self-supported film with a soft shade of brown color, as shown in Figure 2.7b. Mylar turned out to be the best reusable substrate for this method, instead of glass, for its flexibility and smooth surface. These properties ensured the seamless separation of the film. Mylar also has a conductive layer, which proved to be very suitable for the variation of this method described in the following section.
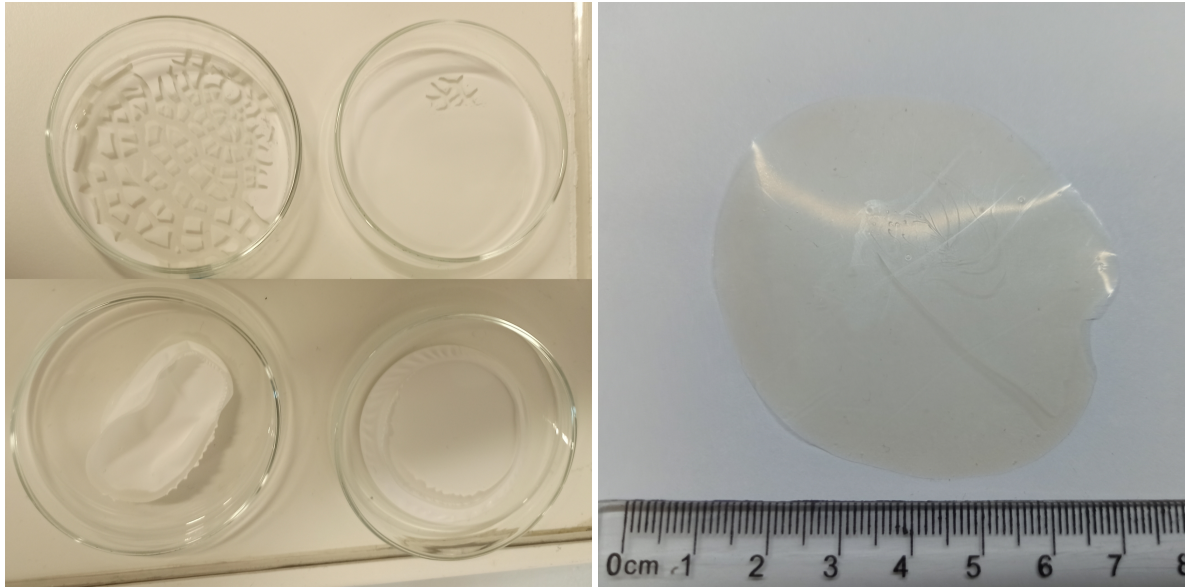
(a) Four samples from the beginning of casting optimization

(b) Successfully cast film photographed on paper for color contrast enhancement

Figure 2.7: Samples prepared by casting method

2.4.1 Curing in electric field

In the process of making ceramic piezoelectric elements, poling is an important step. But since it involves heating up the element this approach can not be used for thermally unstable polymer phases. Yet it was an important inspiration for curing in an electric field. Instead of heating the element, a strong electric field is applied already in the curing stage of the film preparation process. Mylar is a PET film that is coated on one side with a thin layer of aluminum. It is this conductive layer that enables the preparation in an electric field. This way mylar serves both as a substrate and one of the electrodes. For the second electrode, stainless steel perforated sheet was used. 3D printed spacer blocks served well to maintain the correct distance between the electrodes. Phywe power supply provided required high voltage. The whole setup is shown in Figure 2.8. The upper limit for applied electric field turned out to be around $E = 980$ kV·m^{-1}. A stronger field caused emerging of PVDF strings connecting both electrodes. Unlike in electrospinning, such behavior is undesirable here. Usually, it takes around three hours for the PVDF solution to harden enough to be touched without deformation. After that electric field is turned off and spacing blocks are removed. Films are left to completely cure squished between the two electrodes for 24 hours. This is meant to prevent unwanted bending or crumpling.
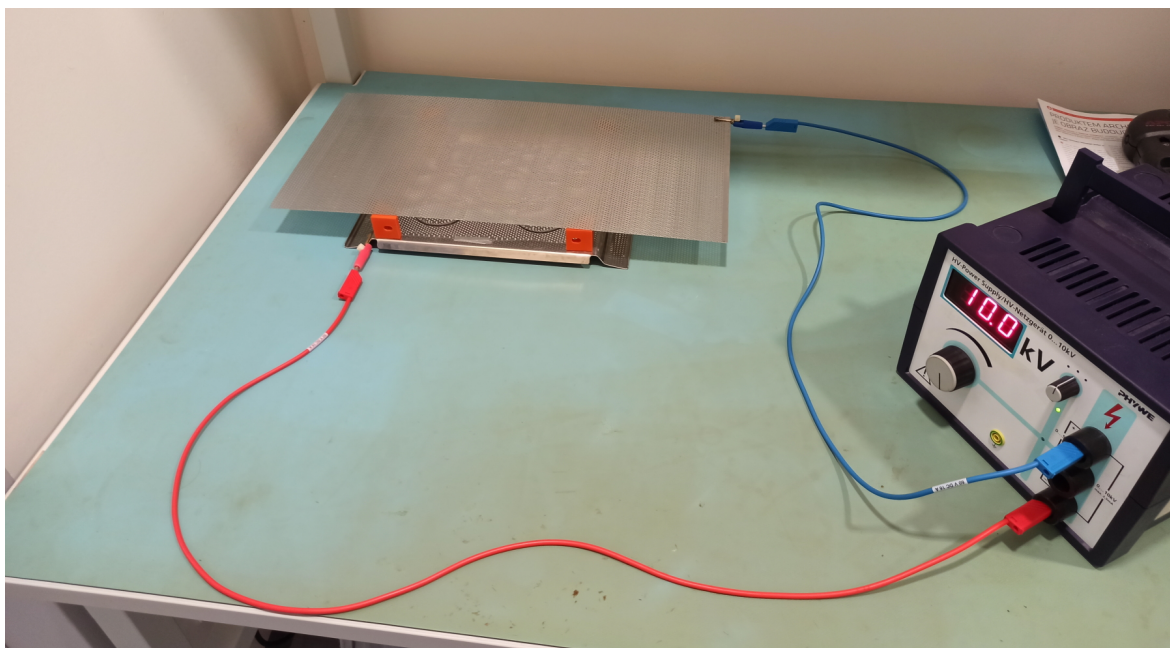
Figure 2.8: Experimental apparatus for curing in an electric field

2.4.2 Spin coating

Spin coating is a well-known method for thin layer preparation. Precursors for this method are always in solution form and there are almost no requirements on the substrate properties. This makes it a perfect candidate for our purposes. Spincoater SPIN 150 with vacuum-mounted glass substrate (flipped Petri dish) was used. Several attempts with different rotation speeds, precursor amounts, and concentrations were performed but none of them was successful. The resulting layers were bumpy with many radial lobes and they were not self-supported enough to be separate from the glass substrate, therefore unusable for energy generator manufacture. Perhaps another approach should have been considered. For example, switching the Petri dish to a mylar sheet would solve the problem of separation. On the other hand, it would complicate the vacuum fixing.

2.5 Water-assisted fast curing

During the aforementioned syntheses, a peculiar behavior of the solution in contact with water was observed (usually in the final cleaning stage of the synthesis). Solution of any used concentration ($c = 5$–$20\,\%$) of PVDF immediately hardened in contact with water. Since PVDF is not soluble in water but both acetone and DMF are miscible with water, the local concentration of solution right at the edge of the phase transition rise above the solubility limit, and dissolved PVDF hardens.

Water-assisted fast curing method takes advantage of this behavior. Here flipped Petri dish served as a substrate. First, a known volume of PVDF solution is measured by a syringe and ejected in the middle of the Petri dish. Then the solution is spread out evenly by tilting or using another smaller Petri dish. Thus formed layer is then submerged in deionized water and kept still for a few dozen seconds. During that time the layer slowly hardens, gains color, shrinks a little, and separates from the Petri dish. Finally, the resulting film is taken out and dried between two sheets of a lint-free wipe.

The result is a self-supported PVDF film of a slightly smaller diameter than the used Petri dish. Films prepared by this method are white in color and can undulate with increasing thickness. A typical result of this method is shown in Figure 2.9.
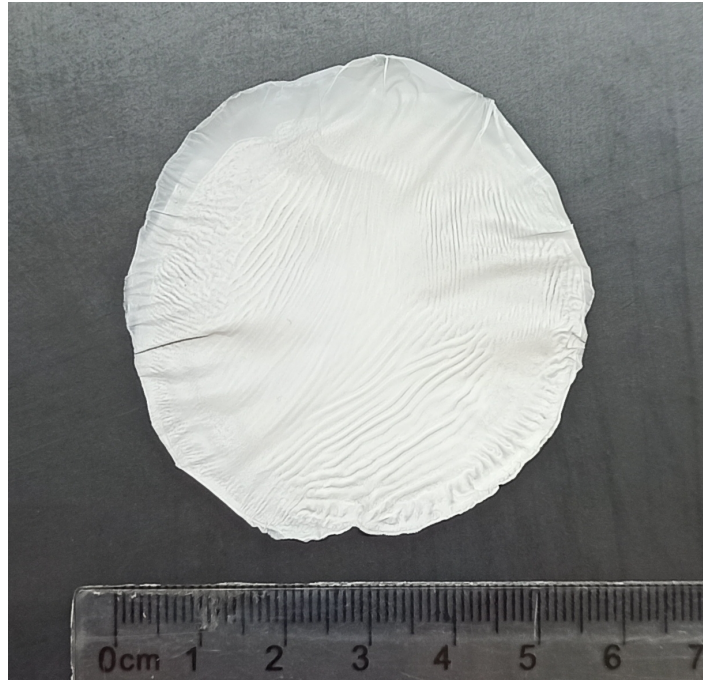

Figure 2.9: A typical result of water-assisted fast curing

2.6 Energy generators manufacture

In the previous chapters, several methods for both self-supported and substrate-supported PVDF layers were described. In order to characterize and compare the piezoelectric properties of the layers thus prepared, energy generators with sandwich-like stricture had to be manufactured. Throughout this thesis the term *generator* is used in the sense of a piezoelectric element designed as a part of an energy harvesting setup (energy harvester). The manufacturing process starts with cutting the polymer layers into a suitable shape. For our purposes, squares of a size 30 mm × 30 mm were chosen. Then electrodes from a thin aluminum sheet ($\tau = (9 \pm 2)$ μm) were attached with sticky copper film. Copper wiring was stuck to this copper film as well. Finally, everything was enclosed in GAG PET foil ($\tau = 250$ μm). Edges of the plastic casing were thermally welded together by squeezing with a hair straightener set to 180 °C for 3 to 4 seconds. The parts before assembling are shown in Figure 2.10a, and a resulting energy generator is shown in Figure 2.10b.

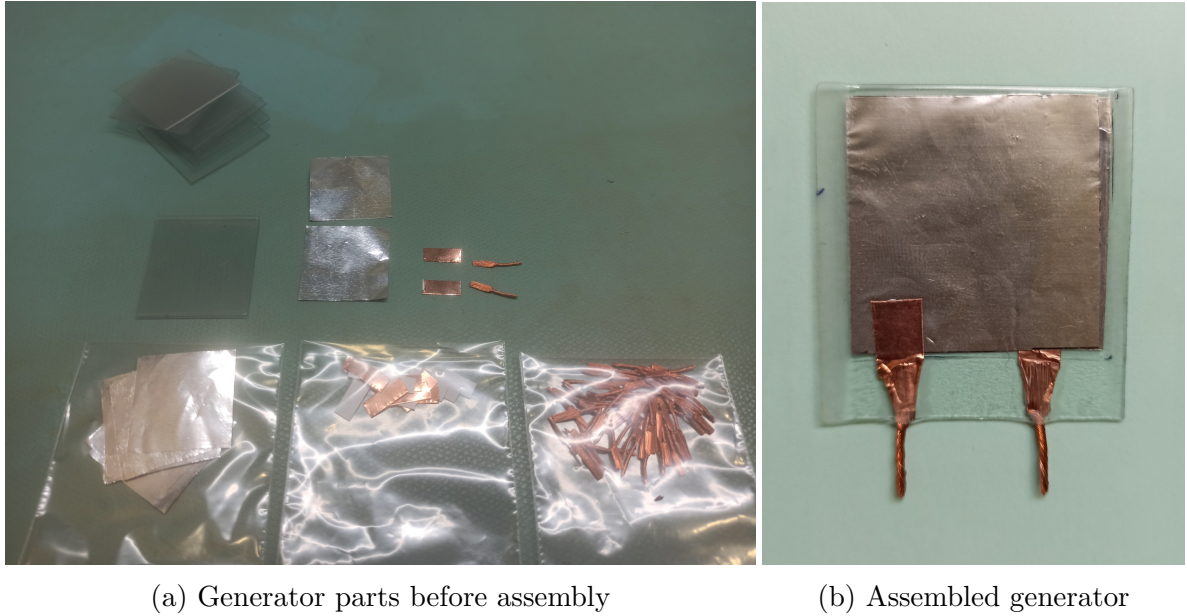(a) Generator parts before assembly   (b) Assembled generator

Figure 2.10: Energy generators before and after assembly process

2.7 Energy generators characterization

The generators manufactured according to the procedure described in the previous section have to be tested and compared, in order to determine which material (method of synthesis) is the most suitable for this application. For this purpose, two parameters were selected and their respective methods of measurement are described in the following sections. Whenever we deal with piezoelectric materials resonant frequency should be in our field of interest. Therefore it is the first parameter and is determined by an impedance analyzer. The second parameter is a peak-to-peak voltage measured with an oscilloscope. Lastly, all generators will be tested in an energy harvesting setup, whether they have the ability to charge a capacitor.

2.7.1 Resonant frequency

A resonant frequency as well as an anti-resonant frequency can be determined by measuring the dependence of the element's impedance on frequency as described in the section 1.2. A resonant and an anti-resonant frequency lies in a local minimum and maximum of said dependence respectively. The impedance of all elements was measured using HIOKI IM 3570 impedance analyzer. In Figure 2.11 a user interface of the impedance analyzer is shown. All measurements were performed on a grounded metal plate to reduce noise. For the same reason measuring speed was set to medium and all points were averaged 5 times. Since the field of interest of this work are low-frequency applications the impedance was measured in a range from 4 Hz[3] to 200 Hz. This impedance analyzer allows the measurement of up to two parameters simultaneously. The second measured parameter was phase angle θ which can also help in finding the resonant frequency.

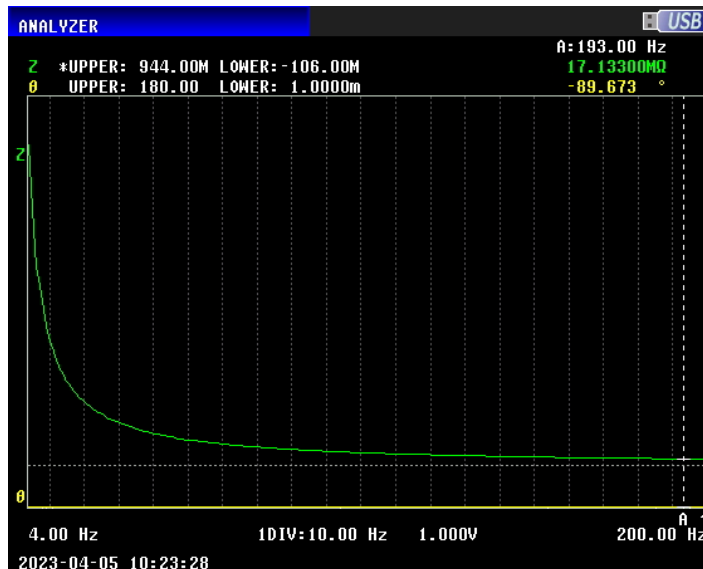[3]The lowest possible frequency for this impedance analyzer.

Figure 2.11: A user interface of HIOKI IM 3570 impedance analyzer

2.7.2 Peak-to-peak voltage

Unlike a resonant frequency peak-to-peak voltage (P–P) is a dynamic property and requires an external stimulus since we are looking at voltage generated in an element by deformation caused by external force. In order to obtain reproducible results well-defined fixing and deformation are needed. For this purpose, a custom holder was designed and 3D printed. The model is available on the author's GitHub [30] together with all other models used and is shown in Figure 2.12 mounted on a ThorLabs XT95 rail. In this figure, the second crucial part of this setup is shown – a magnetic linear motor. The linear motor is controlled by a PI C-413 controller enabling communication between the linear motor and commercial software running on a desktop computer. The motor, the controller, and the software are all provided by Physik Instrumente company as a working setup. The linear motor moves in a range of up to 50 mm. For all measurements performed sinusoidal motion with an amplitude of 20 mm and frequency of 5 Hz was set. For higher frequencies the possible range of motion of the linear motor shrinks. This is a limitation for this method and therefore only measurements at a 5 Hz were performed. More about the linear motor capabilities and limits can be found in [31].

The electrical response of an element was measured using National Instruments PCI-5114 built-in oscilloscope device. This oscilloscope comes with an intuitive user interface shown in Figure 2.13. At the bottom of the screen measurements table is located. In this table, four parameters of interest are displayed: P–P voltage, high and low voltage, and FFT frequency which indeed is 5 Hz just like the motor frequency. This table also shows that all mentioned parameters as well as the recorded plot above are averaged over 128 samples. In order to take advantage of averaging a sophisticated trigger had to be introduced. Since the electrical response of measured elements was not regular enough external trigger signal was needed. For this purpose, one of the programmable output pins of the C-413 controller was used. Through a built-in console, a regular signal was generated on an output pin every time the motor passed a specified position[4]. This signal was then used as an external trigger on channel 1 and

---

[4]and in a specified direction – in order to receive only one pulse per period

28

is shown in blue in the graph. In order to further reduce noise the whole setup was closed in a Faraday cage and signal cables were filtered with a split ferrite core filter.
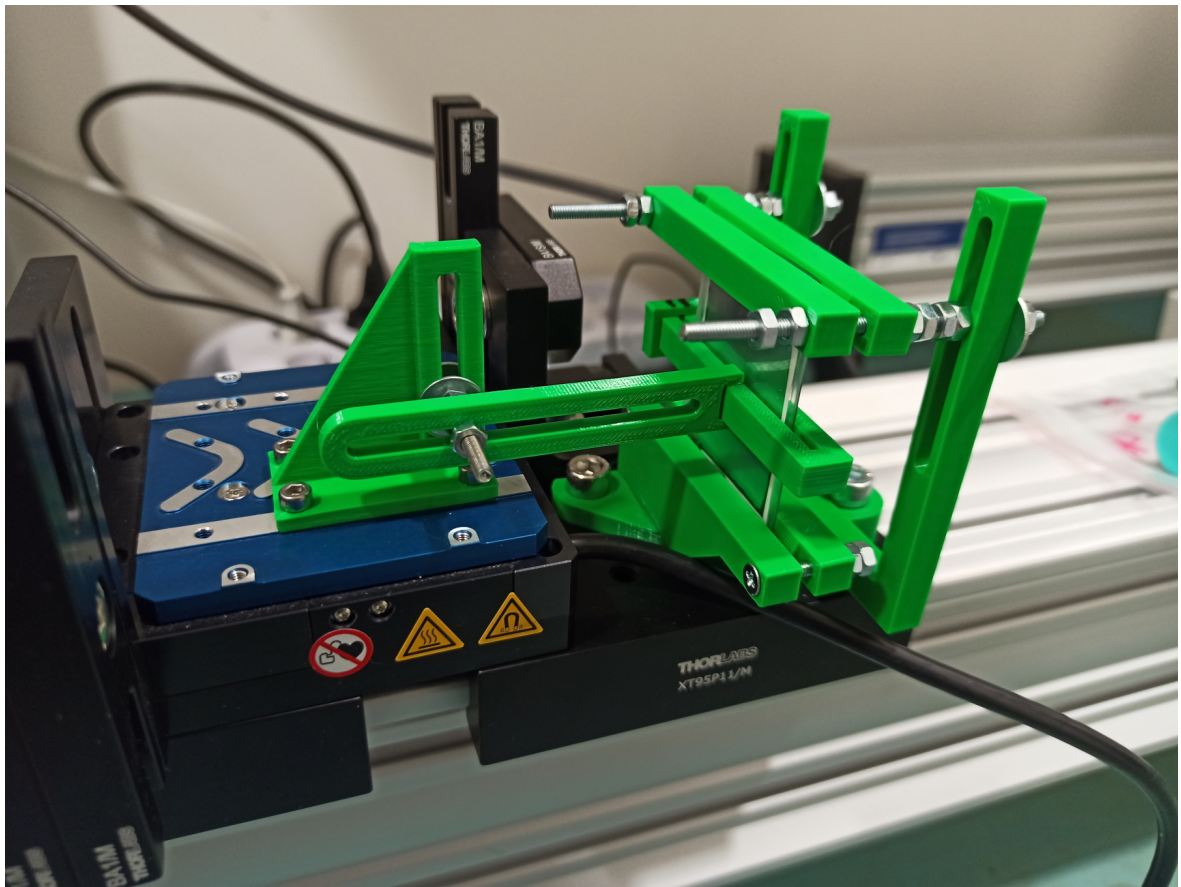

Figure 2.12: 3D printed element holder and linear motor bending setup

Figure 2.13: Oscilloscope user interface

2.7.3 Charging a capacitor

Similarly to the P–P voltage charging a capacitor requires mechanical stimulation, therefore its measuring setup uses the same holder and linear motor mentioned in the previous section. The difference is in the processing of the electric output of the measured element. Instead of using an oscilloscope energy harvester is connected to the element. The circuit used involves an energy harvester LTC3588 and a capacitor. The circuit schematic is shown in Figure 2.14. The energy harvester among other things rectifies and smoothes the current, the capacitor serves as energy storage. The change of voltage on the said capacitor is measured by the oscilloscope described in the previous section. A switchable shortcut is included for a fast discharge of accumulated energy. The measurement itself is done in three steps. First linear motor motion is initiated, then voltage measurement starts, and finally electric shortcut is disconnected. The result is a record of voltage change over time. The desired output for a well-working generator is a steep rise of voltage to the maximum of generated rectified voltage – a half of P–P voltage for a symmetric output voltage (for an asymmetric output max(highest-voltage, −lowest-voltage)).
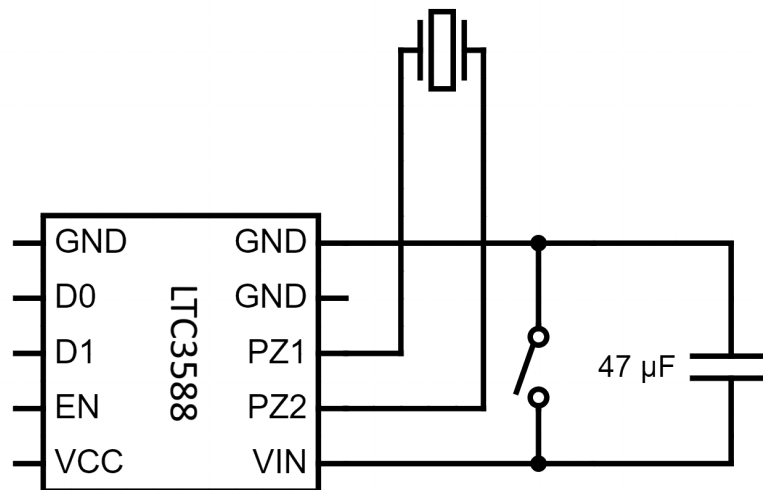

Figure 2.14: Schematic of an electrical circuit for energy harvesting

Chapter 3

Results and discussion

Microstructured polymer layers and piezoelectric energy generators prepared by methods introduced in the previous chapter are described in the following sections. First, polymer films resulting from all methods are presented. Piezoelectric characterization of selected PVDF films is then discussed.

3.1 Electrospinning

The results of the electrospinning method are shown in the following sections. First typical imperfections are described then successfully prepared unoriented and oriented fibers are shown. Finally, a method for analyzing fiber alignment is introduced together with its results.

All samples prepared have a unique sample code. For electrospinning two main tags were given: EU for unoriented and EO for oriented fibers. The second tag describes solution concentration in percentages. The third tag notes the substrate used and the last tag tells the needle-collector distance in centimeters.

3.1.1 Typical imperfections

Before we look at all the imperfections of the prepared samples, let's discuss the parameters that can be used to tune the result. As discussed in the theoretical part of this work the most important parameter is the high voltage. Unfortunately, this parameter is limited to 10 kV by the used hardware. Fortunately, this problem can be circumvented by changing the solution concentration. Three different concentrations were tested $c = 5$ %, 10 % and 15 %. The most concentrated solution was too viscous for the relatively weak electric field used. Thus, no Taylor cone was formed and electrospinning was not possible. On the other hand solution with concentration $c = 5$ % was indeed transferred from the needle to the collector easily but instead of forming long uniform fibers small droplets reached the collector. These droplets were studied using an electron microscope and are shown in Figure 3.1. Their size range from 1 μm to 3 μm. The resulting layers were structurally weak and they couldn't resist even a slight touch. Therefore they were not very suitable for generator manufacture.

HV	curr	WD	det	HFW	PW	30 µm
30.00 kV	47 pA	12.7 mm	ETD	78.5 µm	25.6 nm	

Figure 3.1: Result of electrospinning solution with concentration $c = 5\,\%$ under a SEM

Solution with concentration $c = 10\,\%$ performed by far the best of the three tested. Well-defined fibers with a narrow size distribution were obtained. Hence this concentration was used for all subsequent electrospinning syntheses. SEM images of said fibers are shown in the following sections in Figures 3.8 and 3.11. Nevertheless, this concentration is not quite optimal and other parameters will need to be adjusted to obtain a perfect product. Two typical imperfections occurred in samples made from a solution of this concentration and are shown in Figure 3.2 and 3.3. These are two types of droplets. The first type is small droplets which are part of one or more fibers. The second type is large droplets that are spread out on the substrate. The frequency of these imperfections is related to the distance of the needle from the target. This dependence is discussed in the following section.

In Figure 3.3 element analysis of a big droplet is shown. The upper left part is a SEM BS electrons image. The big droplet is the dark circular spot approximately 140 μm in diameter. The remaining images are combinations of this gray-scale image and an EDS map of a selected element. This sample uses an aluminum sheet as the substrate, therefore a lot of signal is detected everywhere except the big droplet. Since EDS uses a bigger interaction volume than BS SEM, the signal from aluminum is received from fibers and small droplets as well[1]. Fluoride in yellow and carbon in pink shows presence in the opposite areas. Both, especially the fluoride, perfectly map areas with fibers and small droplets. The big droplet is colored pink and yellow as well. This confirms that we are indeed dealing with a locally deposited thin layer of PVDF.

An observant reader may notice three abnormally shaped chunk of material which is highlighted in pink but not in yellow. In other words, it contains carbon but no fluoride. The exact origin of these particles is unclear but the most probable explanation is airborn contamination.

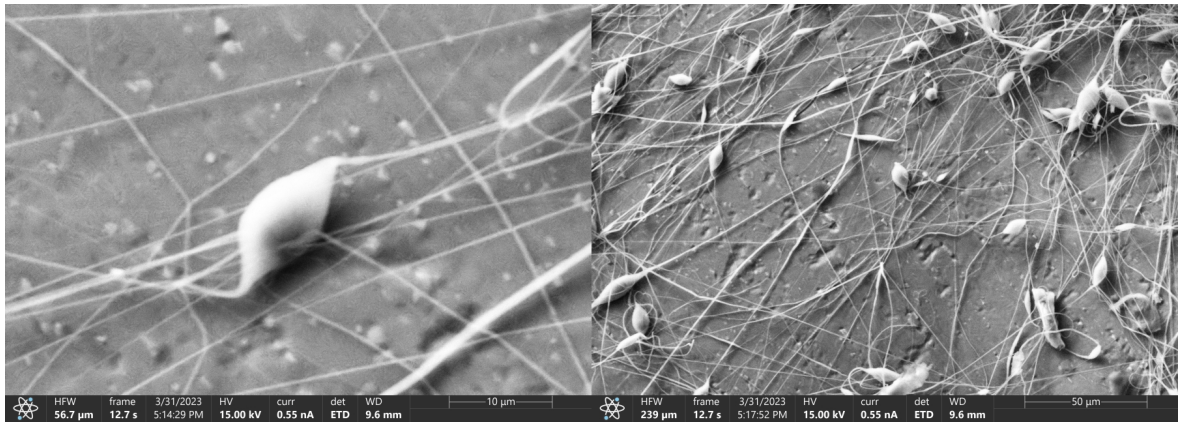[1]EDS looks "underneath" them as well.

Figure 3.2: Small droplets connected to one or multiple fibers – imperfection
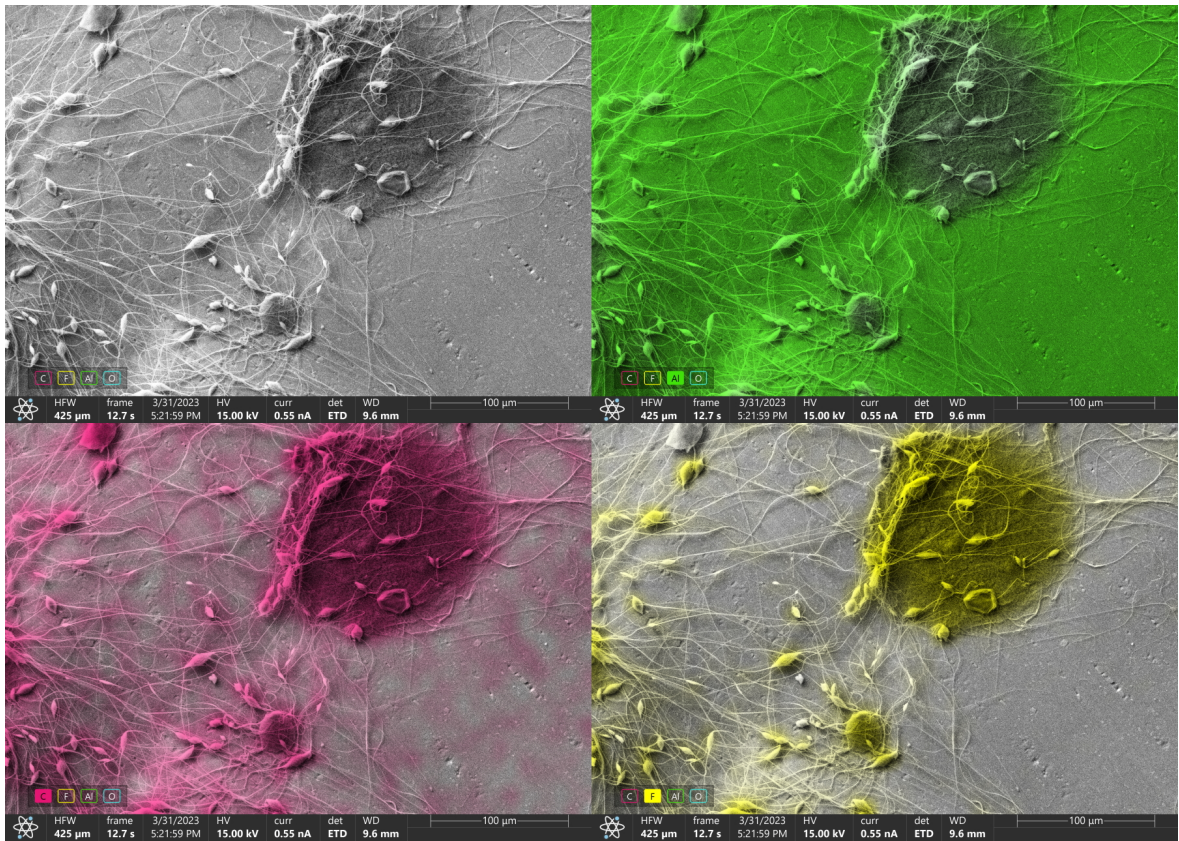
Figure 3.3: Element analysis of big droplet imperfection (gray-scale – BS electrons, green – aluminum, pink – carbon, yellow – fluoride)

3.1.2 Distance and flow rate

An optimal needle–collector distance is a distance at which there is a constant flow of material between the needle and collector. If the distance is too short, regular fast bursts of material towards the collector can be observed. On the other hand, too long distance causes accumulation of the material at the needle tip followed by regular dripping which breaks the needle–collector material flow. Both of these scenarios are unwanted since they cause imperfections in the product. The optimal needle–collector distance was measured for a range of flow rates from 0.5 ml·h^{-1} to 4 ml·h^{-1} for two different concentrations $c = 5$ % and 10 % on the both static and rotating collector.

Two plots showing ranges of possible distances for a given flow rate are shown in Figure 3.4. The upper plot shows this dependence for a static collector. The ranges of the two concentrations overlap each other and in both cases, the optimal distance is inversely proportional to the flow rate. This is caused by the change in electric field. The high voltage was set to 10 kV for all measurements but the electric field was proportional to the distance. Therefore higher flow rates require a smaller distance – a stronger field. In the second plot, the same dependence is shown for the rotating collector. Here ranges are not overlapped rather the 10 % concentration required smaller distances. This is again a reasonable behavior. Higher concentration means higher viscosity therefore stronger field is needed to create a Taylor cone and maintain material flow.

It should be noted here that the uncertainty in the measurement of the optimum distance is large. The evaluation method consisted of slowly changing the distance periodically and observing whether the material flow was stable. This method often brought different results for the same combination of parameters since we are dealing with a dynamic system on the edge of its stability. The resulting plot represents a weighted mean of the obtained results.
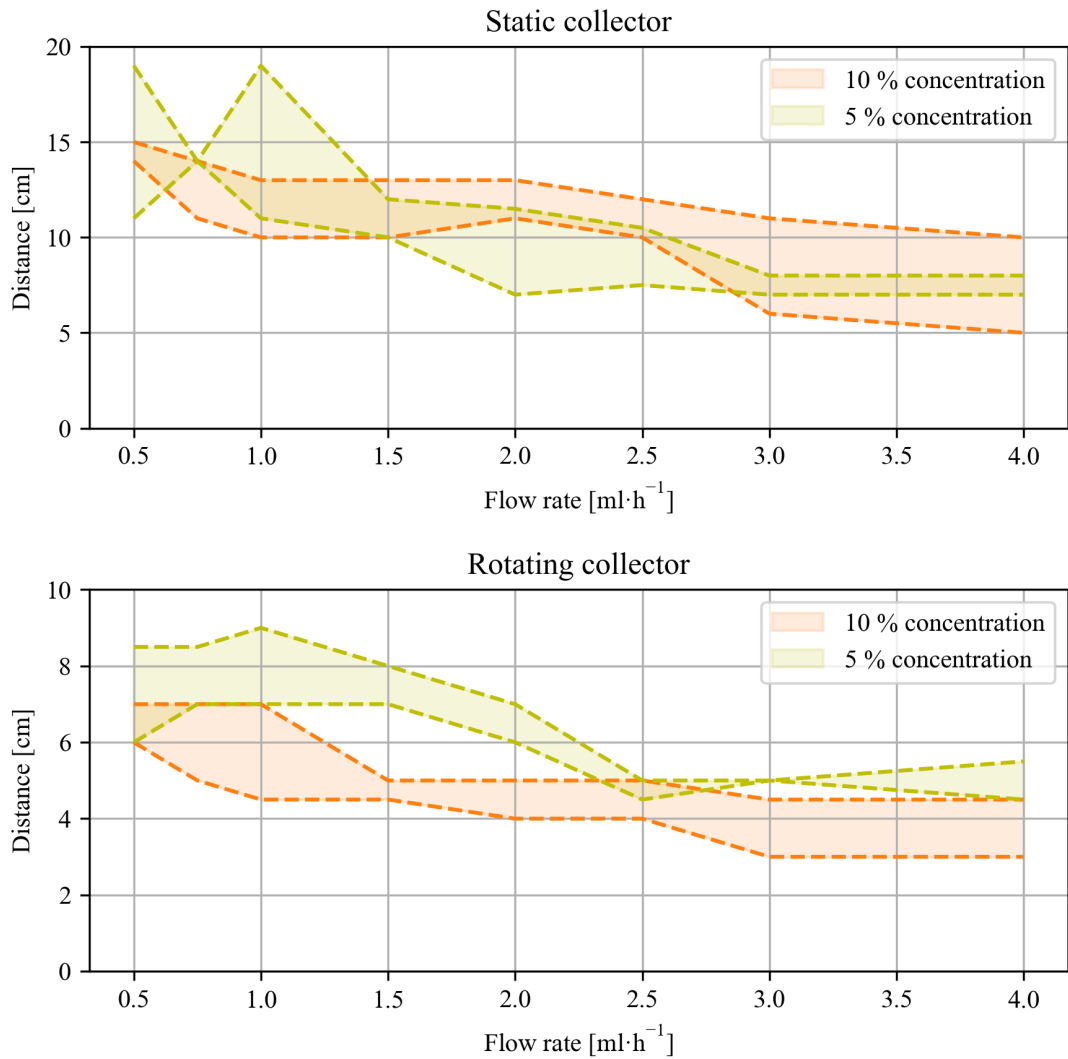

Figure 3.4: Optimal needle–collector distance for selected flow rates tested for both static and rotating collector
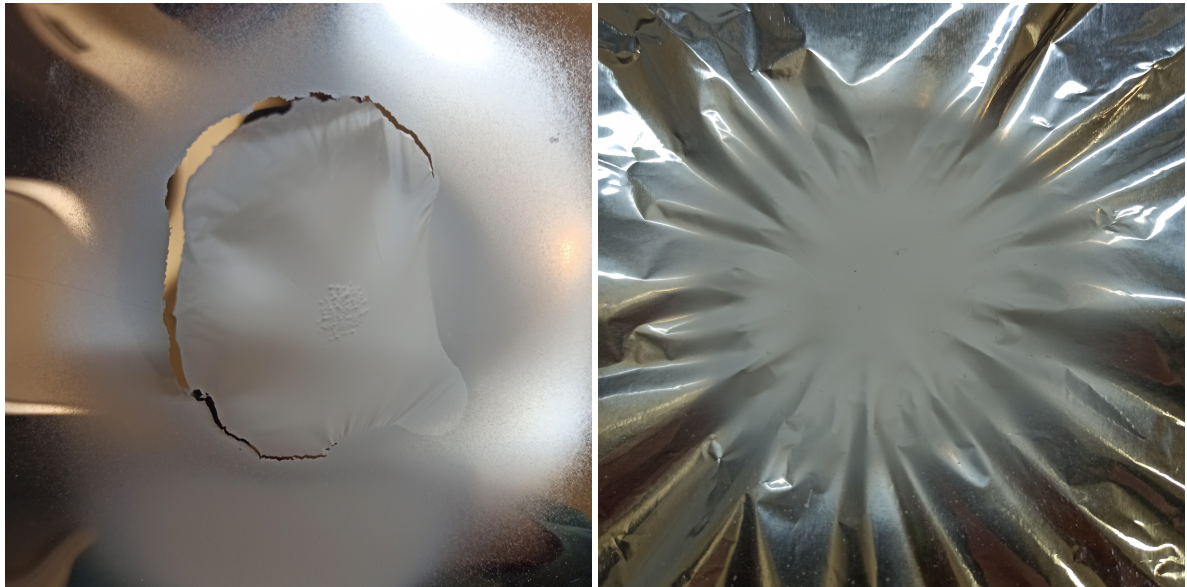
3.1.3 Unoriented fibers

In previous experiments, the 10% solution proved to be the most optimal. Therefore ten different samples were prepared using this concentration. Four samples were deposited on mylar and four were deposited on aluminum foil with different needle-collector distance $d = 8$, 10, 12, and 14 cm. All of them were deposited for 30 minutes with flow rate $Q = 1$ ml·h^{-1}. The last two samples were deposited on mylar and aluminum foil with the same flow rate for three and a half hours. All the samples were suitable for generator manufacture except EU_10_M_14[2]. In the case of this sample, deposition resulted in multiple weakly connected layers rather than just one compact layer.

In Figure 3.6 SEM images of four samples are shown. In the left part, it can be seen that needle-collector distance does not affect fiber diameter in the used range. In all four samples fibers with diameters approximately from 100 nm to 600 nm are present. On the other hand quantity and nature of imperfections strongly depend on the distance. With increasing distance number of small droplets quickly decreases and the number of big droplets increases. This phenomenon can be seen in the right part of the image.

Radial thickness of a deposited layer was measured for two samples with long deposition time (3:30 hours) and is shown in Figure 3.7. The highest thickness is in the middle of the samples and is decreasing with increasing distance from the center. This is an expected behavior but the curve shape was expected to be more rectangular (sample on mylar target) than linear (sample on aluminum target). Uncertainty of this measurement is in order of tens of μm because the layers can be squished by the micrometer during measurement.

Also, it is important to note here that longer deposition caused some problems. A drying layer tends to shrink. After long deposition samples on mylar tore up as shown in Figure 3.5a because the substrate is too rigid. On the other hand, samples deposited on aluminum foil crumpled as shown in Figure 3.5b.

(a) Long deposition on mylar   (b) Long deposition on aluminum

Figure 3.5: Samples deposited for three and a half hours with flow rate $Q = 1$ ml·h^{-1}

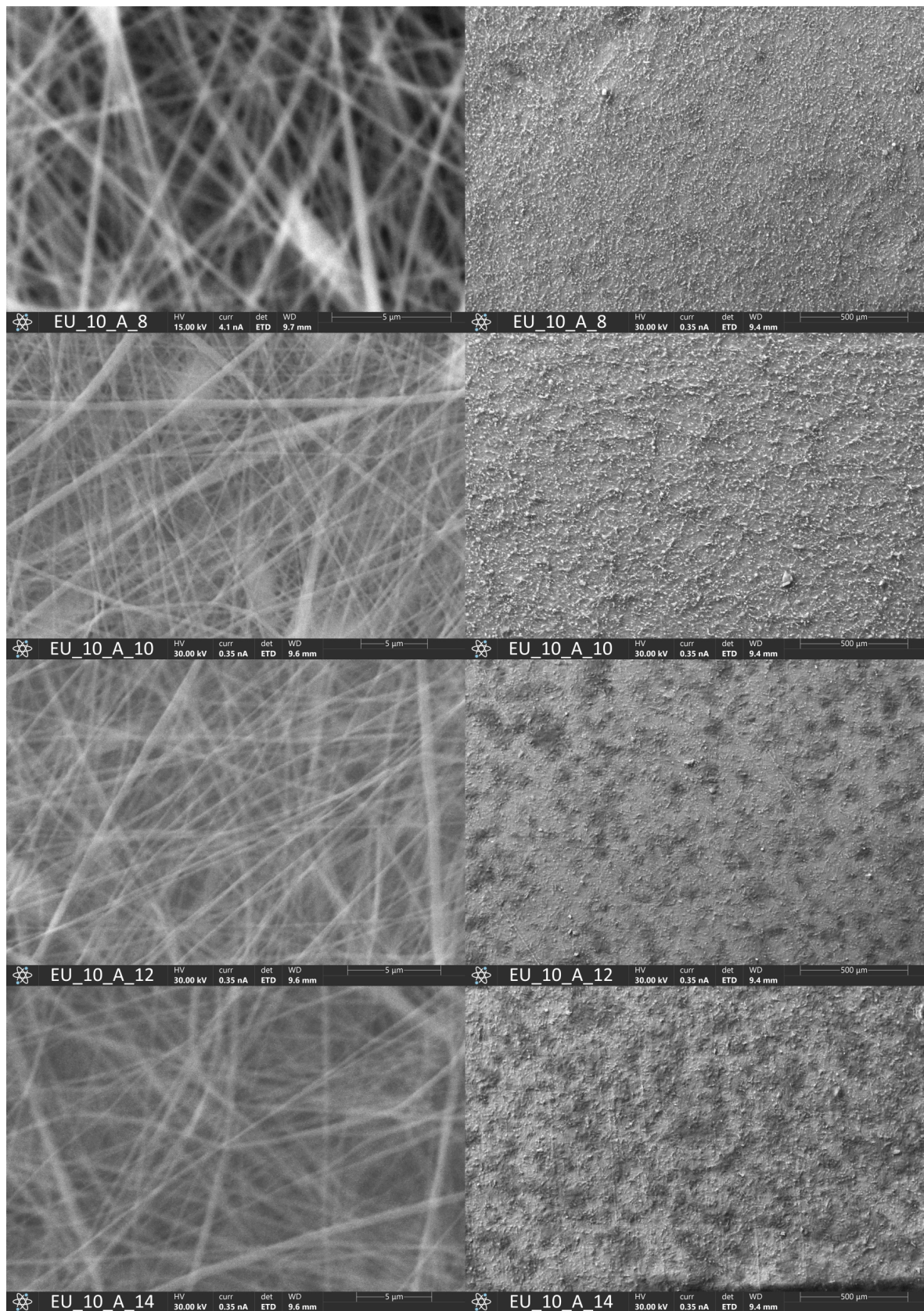[2]electrospun unoriented fibers – 10% concentration – deposited on mylar – 14 cm needle-collector distance

Figure 3.6: SEM images of samples prepared from solution with 10 % concentration of PVDF deposited on aluminum foil using static collector in different distances. Sample code: EU – electrospun unoriented fibers, 10 – % concentration, A – deposited on aluminum, 8–14 – needle-collector distance in centimeters
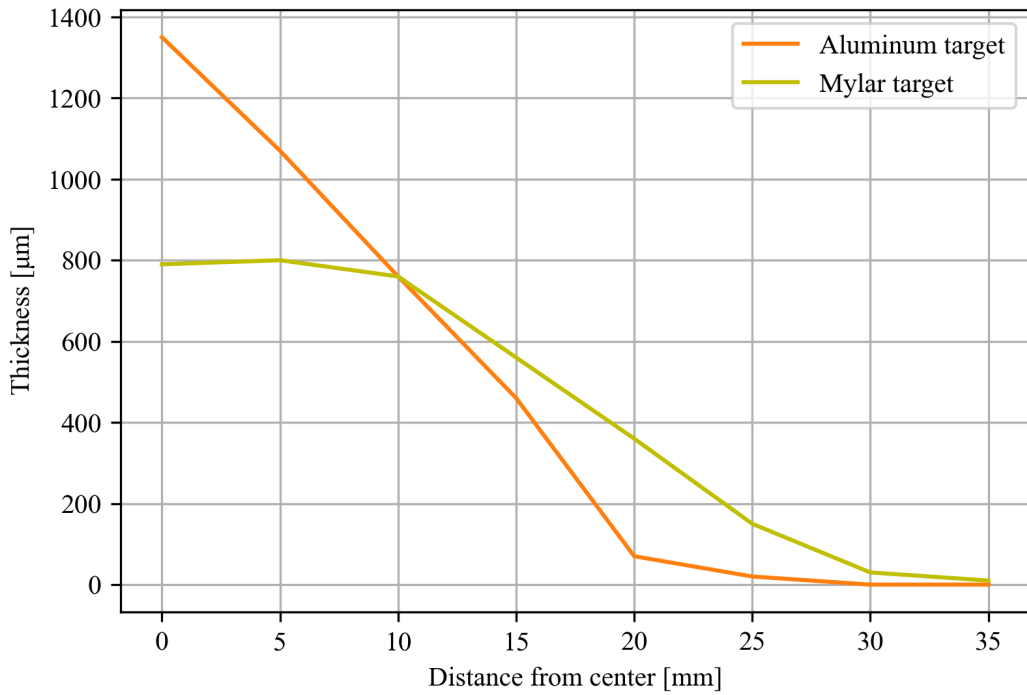
Figure 3.7: Radial thickness of two samples deposited for 3 and a half hours on mylar and aluminum foil. Solution with concentration $c = 10$ % and static collector in a distance of 10 cm were used.

3.1.4 Oriented fibers

For all samples prepared on a rotating collector 10% solution of PVDF was used. As shown in Figure 3.8 result is again well-defined fibers with diameters ranging approximately from 50 nm to 400 nm. But this time vertical orientation is strongly preferred. Only a small number of fibers is completely misaligned. A degree of alignment is discussed in detail in the following section.
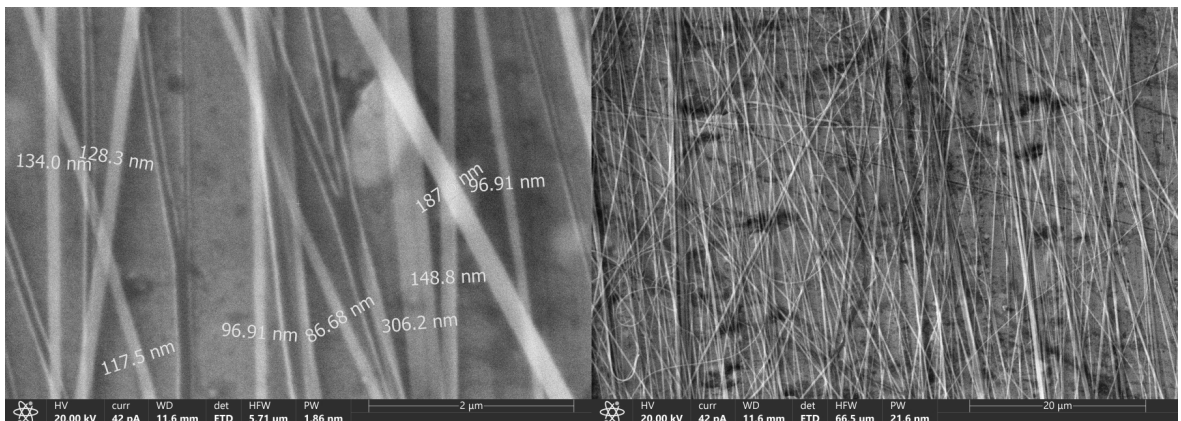
Figure 3.8: SEM BS electrons image of oriented fibers

A photo of a sample after removal from the rotating collector is shown in Figure 3.9. It's clear that the thickness of the deposited layer is bigger on one side even though the collector is aligned with the needle perfectly. A possible explanation for

37

this behavior is an unevenness in charge distribution since high voltage is conducted to the substrate by copper wires leading from the center of the collector to only one side of the substrate. The side with a thicker deposited layer is just this side.

From Figure 3.9 it is also clear that mylar is not a suitable substrate for this method. When removed from the collector, the mylar unwinds, and the deposited layer breaks. Therefore only aluminum foil was used. Two generators were prepared from a sample with oriented fibers. For both of the generators, the same sample was used. The only difference is the orientation of the fibers. The generators were manufactured in such a way that the sample was rotated 90 degrees in the second generator.
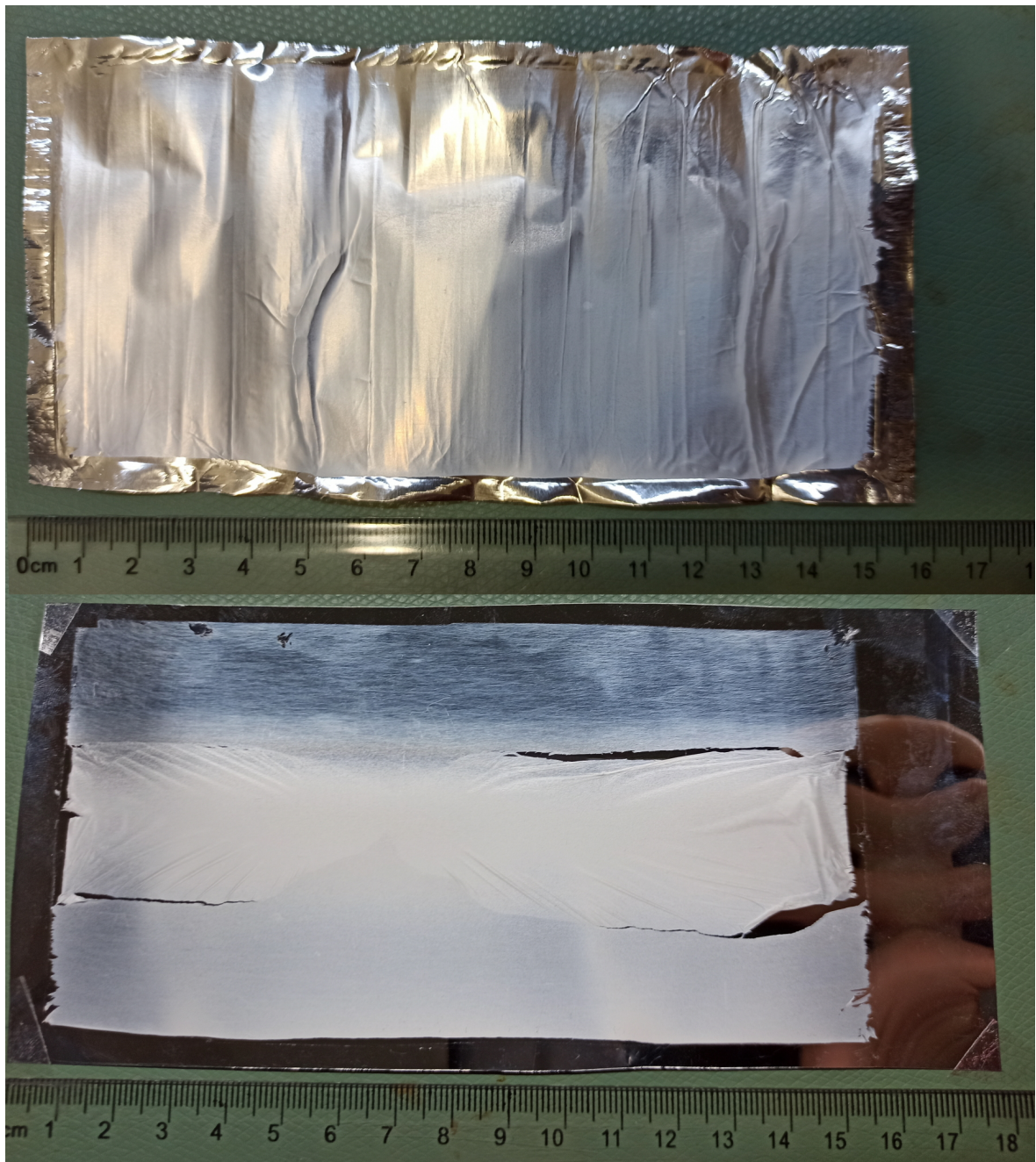
Figure 3.9: Photo of a sample after removal from the rotating collector on aluminum foil (top) and mylar (bottom)

Alignment analysis

With the creation of aligned fibers the need for a reproducible method for alignment analysis emerged. For this task python environment was selected with a help of openCV library[3].

Images acquired using SEM were processed in the following steps:

1. Loading raw grayscale image,

2. Equalizing the intensity histogram,

3. Pre-blurring the image,

4. Detecting edges using openCV Canny method,

5. Detecting lines using openCV Probabilistic Hough Line Transform,

6. Calculating and displaying angle distribution in a polar histogram.

The resulting images after a selected steps of the alignment analysis are shown in Figure 3.10. Analyzed sample with fibers oriented in one direction is shown in Figure 3.11 together with angle histogram distribution clearly showing a strong dominance of this direction. It is important to note here that the angles are calculated relative to the horizontal direction, symmetrical angles (respective to the chosen angle range) are considered identical and most importantly the histogram shows a distribution of angles of lines found not fibers therefore it is normalized.
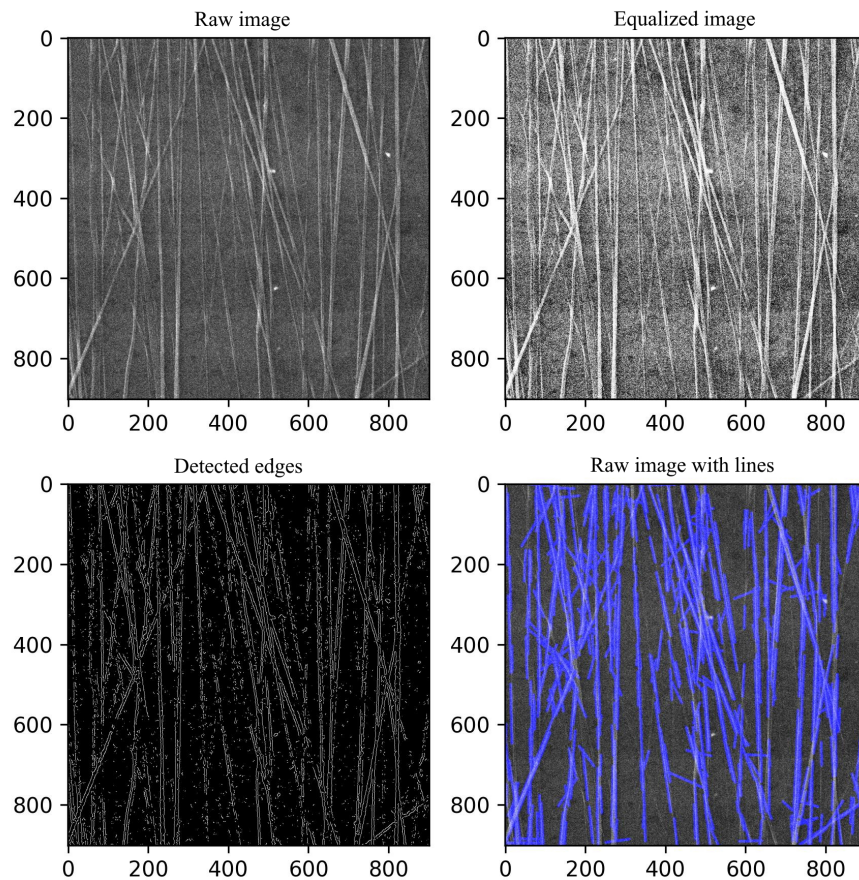
Figure 3.10: Image after selected steps of the alignment analysis.

---

[3]open source computer vision library
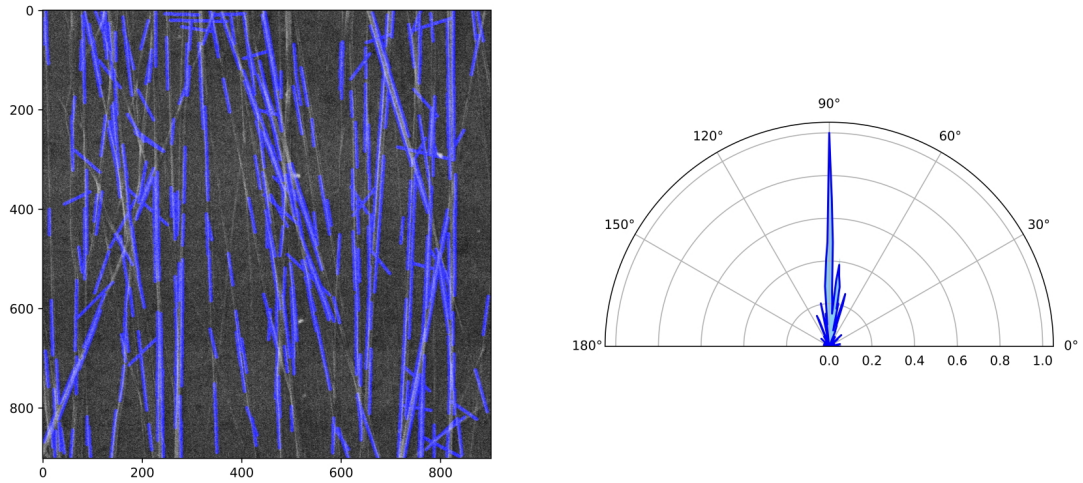
Figure 3.11: Image of aligned fibers with highlighted edges and polar histogram of the relative number of edges found

After a successful deposition of fibers aligned in one direction, an attempt to deposit a rectangular grid was performed. The result is shown in Figure 3.12 after an alignment analysis. In the histogram two dominant orientation directions are clear. Therefore proving the great potential of this method for future research beyond the scope of this work. An example would be applications related to filters.
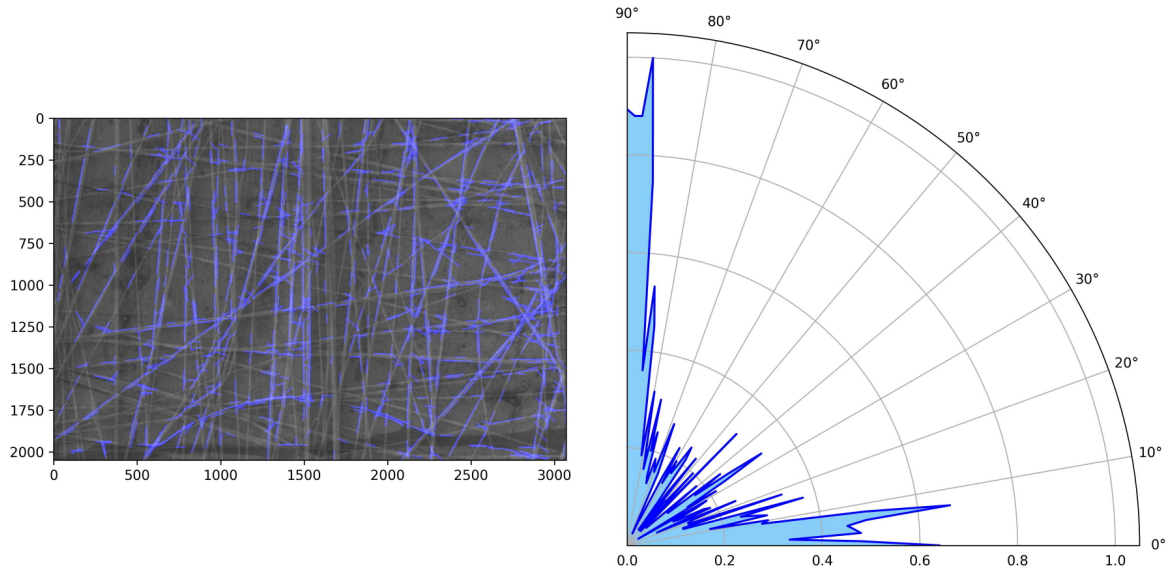
Figure 3.12: Image of fibers aligned in a square grid with highlighted edges and polar histogram of the relative number of edges found

It should be noted here that image analysis is not the author's field of study therefore this method has plenty of room for improvement. For example, the usage of a suitable combination of dilatation and erosion or another method for noise reduction like small cluster filtration could be considered.

3.2   Casting

Using the casting method described in the section 2.4 five different samples were prepared. For all of them, 20% solution of PVDF and mylar substrate was used. They differ in the electric field applied during curing. In the table 3.1 all samples with their respective applied electric fields are shown. The nature of this method allowed the preparation of either one large sample or up to four smaller samples still suitable for generation manufacture. The second approach was used, therefore the result is four films prepared identically and thus having the same sample tag. Sample tags for casted samples start with C. The second tag is a serial number. The difference between samples C_2_A and C_2_B is in the method used for spreading the material. Sample A was spread by gravity, sample B was spread using a laboratory spoon. This difference affected both thickness (shown in the table 3.2) and film separation from the substrate (separation of the B sample was impossible).

Sample code	$d = $ [mm]	$U = $ [kV]	$E = $ [kV·m^{-1}]
C_1	–	0	0
C_2_A	27	10	370
C_2_B	27	10	370
C_3	20	10	500
C_4	10	9.8	980

Table 3.1

Samples separated from mylar are shown in Figure 3.13. All samples are transparent with a soft shade of brown color. In some samples imprint of the upper electrode is visible. This has no effect on the sample properties since it only influenced the uppermost layer of the sample. Some samples have white stripes which probably originated during the pouring process. All of the five samples (including the C_2_B not shown in Figure) were suitable for generator manufacture.
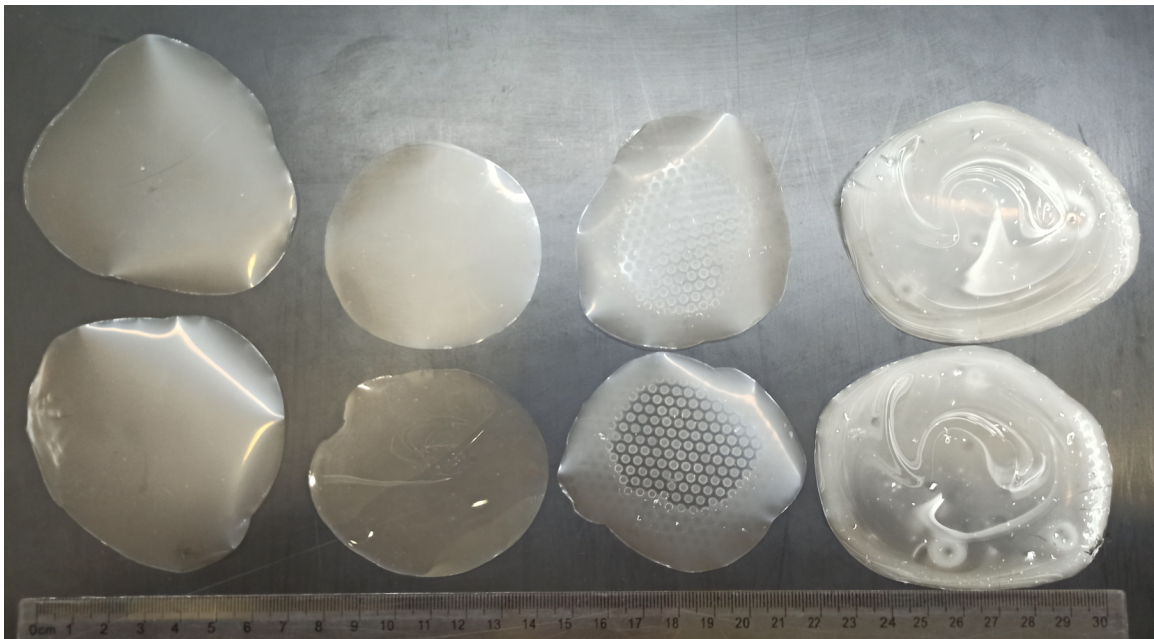
Figure 3.13: Casted samples separated from mylar substrate. From the left: C_1, C_2_A, C_3, C_4

3.3 Water-assisted fast curing

Using the water-assisted curing method 17 samples were prepared. Results are thin self-supported films and are shown in Figure 3.14. All the samples are white and opaque and are undulated or warped to some degree. All of them are suitable for generator manufacture but only four of them were selected – one sample of each solution concentration so that they have all approximately the same thickness. All the respective thicknesses and whether the sample was selected for generator manufacture are shown in the table 3.2. A sample code for water-assisted curing starts with H. The second tag is again the concentration in percentages. The last tag is the volume of solution in milliliters used.

Figure 3.14: All samples prepared by water-assisted curing

3.4 Amorphous or crystalline

As explained in the section 1.1 we are not dealing with completely amorphous nor crystalline polymers but rather a combination of both – semicrystalline polymers. The question to be asked is how the preparation method affects the degree of crystallinity. If we look at the casting method and water-assisted curing judging only by the nature of the methods it is reasonable to expect the casting method to result in a layer with a higher degree of crystallinity since the curing process is very slow and therefore provides better conditions for the formation of crystalline domains. Fast water-assisted curing on the other hand forces the material to harden immediately into a more chaotic state.

Now considering the optical properties of prepared films it would be natural to say that casted films are more crystalline since they are almost transparent and transparency goes hand in hand with high crystallinity when dealing with inorganic materials like minerals. In the case of semicrystalline polymers formation of large[4] crystalline domains causes scattering leading to transparency deterioration [32].

In order to measure the actual degree of crystallinity of prepared PVDF layers X-ray diffraction could be used.

3.5 Measured generators

Using the method described in the section 2.6 17 generators were manufactured from PVDF films selected based on the method used and their suitability in terms of shape, size, thickness, and first of all imperfections like holes, undulation or warping. In the following sections, their piezoelectric properties are presented and their suitability for energy harvesting is discussed.

For all measurements performed on the generators, a reference generator was measured as well. The reference generator is manufactured the same way as all the others with a LDPE film in the middle instead. This allows comparison and evaluation of the piezoelectric effect.

3.5.1 Thickness

The thickness of all samples was measured using a digital micrometer and all the results are shown in the table 3.2. The uncertainty of these measurements has two parts. The first is the uncertainty of the measuring device itself, which is $\delta = \pm 0.002$ mm. The second part is the uncertainty caused by elastic deformation of the measured film during measurement. This uncertainty was different for all the methods of preparation with the highest being approximately 5 % of the measured value for electrospun samples. Also, the thickness varies on different spots on a single sample. For electrospun samples radial thickness was discussed at the end of the section 3.1.3. The thickness of the casted samples as well as the samples prepared by water-assisted curing behaved far more randomly rather than monotonously decreasing from the center. Therefore multiple measurements were performed for each sample and the result is a range, not a single thickness. For many of the samples, the color shade led to a quick finding of the both thinnest and thickest spot.

---

[4]similar or bigger than a wavelength of light

Sample code	$\tau = [\mu m]$	generator made
Reference	40	yes
EU_10_M_8	35–140	yes
EU_10_M_10	20–130	yes
EU_10_M_12	15–80	yes
EU_10_M_14	immeasurable	no
EU_10_M_10_L	10–790	yes
EU_10_A_10_L	20–1350	yes
EU_10_A_8	15–25	no
EU_10_A_10	20–40	no
EU_10_A_12	20–90	no
EU_10_A_14	10–50	no
EU_5_A	immeasurable	no
EO_10	7–9	two orientations
EO_5	3–5	yes
C_1	80–105	yes
C_2_A	110–160	yes
C_2_B	40–80	yes
C_3	80–100	yes
C_4	100–120	yes
H_5_10	80–160	no
H_5_08	80–150	no
H_5_06_A	30–110	yes
H_5_06_B	20–60	no
H_5_05	20–40	no
H_5_04	8–30	no
H_10_10	80–160	no
H_10_08_A	40-60	yes
H_10_08_B	60–110	no
H_10_06	20–40	no
H_15_12	30–80	yes
H_15_10	30–60	no
H_15_08	20–50	no
H_15_06	25–40	no
H_20_08	40–60	yes
H_20_06	20–60	no
H_20_04	20–30	no

Table 3.2: Table of all samples, their thicknesses, and whether a generator was manufactured. The thickness of two samples was immeasurable because the layer was not resistant to touch.

3.5.2 Impedance analysis

All manufactured generators were analyzed using an impedance analyzer. Frequency dependency of an impedance Z and phase angle θ of all generators including the reference generator are shown in Figure 3.15 and 3.16 respectively. Despite expectations, there are no peaks typical for piezoelectric behavior present in measured data. Rather,

all generators act like a typical capacitor. The generator's sandwich structure resembles a capacitor arrangement. When dealing with capacitors we can focus only on capacitance. Frequency dependency of the capacitance of a capacitor is described as follows

$$X_\mathrm{c} = \frac{1}{2\pi f C}.$$ (3.1)

By fitting the measured data with this function capacity of all generators can be calculated. Thus obtained capacities are shown in the table 3.3. Generators manufactured from films prepared using the same method exhibit capacities in a similar range. It is also clear that the capacity of each generator strongly depends on the film thickness the same way as when dealing with regular capacitors. A capacity of a parallel plate capacitor can be calculated using this formula

$$C = \frac{\epsilon_\mathrm{r}\epsilon_0 A}{d},$$ (3.2)

where A is the plate area, d is their distance, ϵ_r is relative electric permittivity and ϵ_0 is electric permittivity of a vacuum. Here it is clear that capacity is inversely proportional to the distance d in our case film thickness τ. Therefore generators from layers of electrospun oriented fibers being the thinnest result in the highest capacity. On the other hand, long deposition electrospun films are the thickest and accordingly result in generators with the smallest capacity. Films of unoriented fibers are thicker than films of oriented fibers and also make generators with smaller capacities. Casted films and films prepared by water-assisted curing result in generators with similar capacities and also have similar thicknesses. All these results are consistent with the theory.

Using the formula 3.2 theoretical capacity of the generators can be calculated. Although one assumption has to be made – the relative permittivity of prepared films. According to [33] the relative permittivity of PVDF fibers is $\epsilon_\mathrm{r} = 2.1$. Considering this we get $C \approx 17$ pF for $\tau = 1$ mm which is consistent with the capacity of thick long deposited films. For $\tau = 10$ μm calculated capacity is $C \approx 1670$ pF. This is much higher than the capacity measured for the thinnest generators. This is caused by tight air gaps between the individual layers of the generators effectively lowering the capacity. Especially thick air gap caused a small capacity for reference as well.

Also in both figures 3.15 and 3.16 increased noise around 50 Hz is visible. This noise is caused by surrounding electronics and it is no coincidence that it is the strongest at 50 Hz since it is the frequency of the electrical grid.
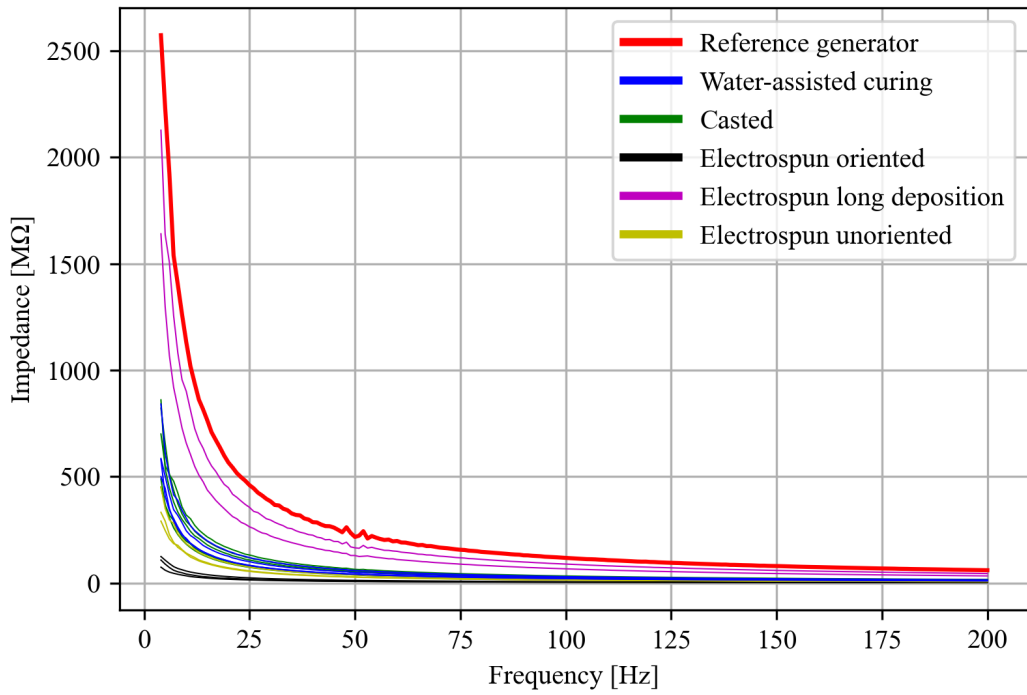
Figure 3.15: Frequency dependence of the impedance Z of all generators
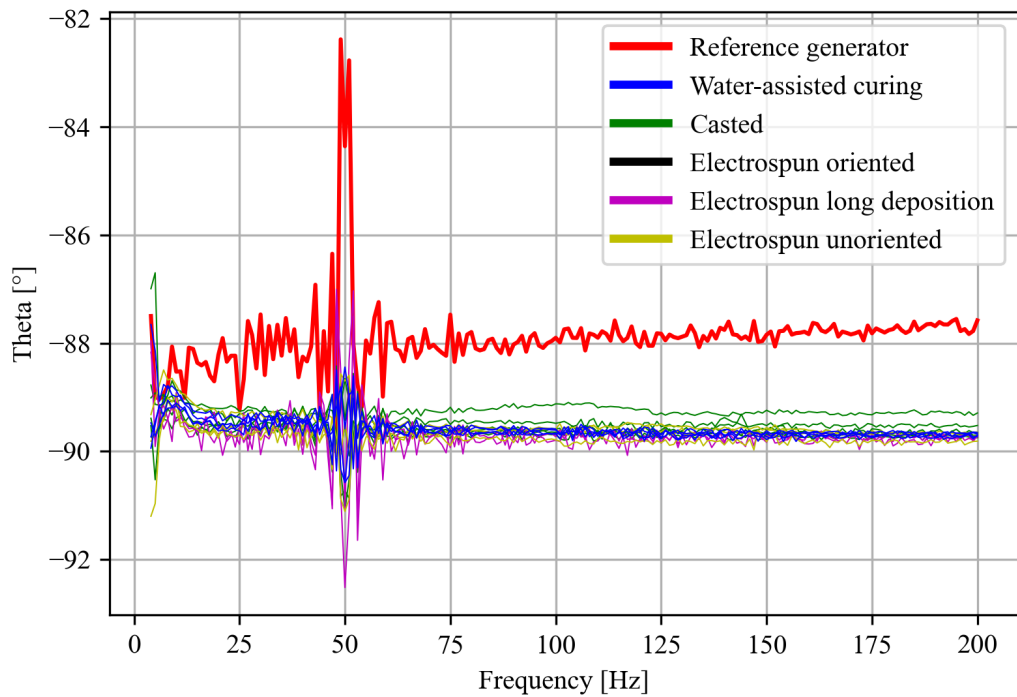
Figure 3.16: Frequency dependence of the phase angle θ of all generators

Sample code	$C = $ [pF]
Reference	14
C_1	49
C_2_A	55
C_2_B	56
C_3	81
C_4	87
EO_10_H	289
EO_10_V	492
EO_5	369
EU_10_A_10_L	18
EU_10_M_10_L	24
EU_10_M_8	116
EU_10_M_10	87
EU_10_M_12	121
H_5_06_A	65
H_10_08_A	75
H_15_12	52
H_20_08	77

Table 3.3: Table of respective capacities of all generators calculated from impedance analysis

3.5.3   Peak to peak voltage

Electrical response on a periodic deformation was measured by an oscilloscope for all the generators and a one second record is shown in Figure 3.17. The electrical response of the reference generator is shown colored in red for comparison. It is clear that some of the generators performed many times better than the reference.

In Figure 3.18 characteristic values for all generators are shown in comparison with the reference baseline. The upper plot shows P–P voltage and the bottom plot shows both maximum high and low voltage for all generators. Here it is clear that all of the generators except H_15_12 performed better than the reference. The best perform- ing generator was C_3 with $U = 95.7$ mV. This result is unexpected and difficult to explain considering the sample being in the middle of a series of samples. A monotonic trend was rather expected.

Films prepared using water-assisted curing generally performed the worst of all methods. This could indicate a lower degree of crystallinity. Films prepared by other methods performed similarly with surprisingly big differences between similar samples. This could be caused by small changes in mounting. Even though it was designed to be as reproducible as possible. It is well known that the way of fixing a piezoelectric element in place strongly influences the measured result. The last thing to notice here is that the electric response was symmetric for all the generators.

For all the generators periodic signal with a frequency of 5 Hz was observed which is consistent with the frequency of the linear motor.
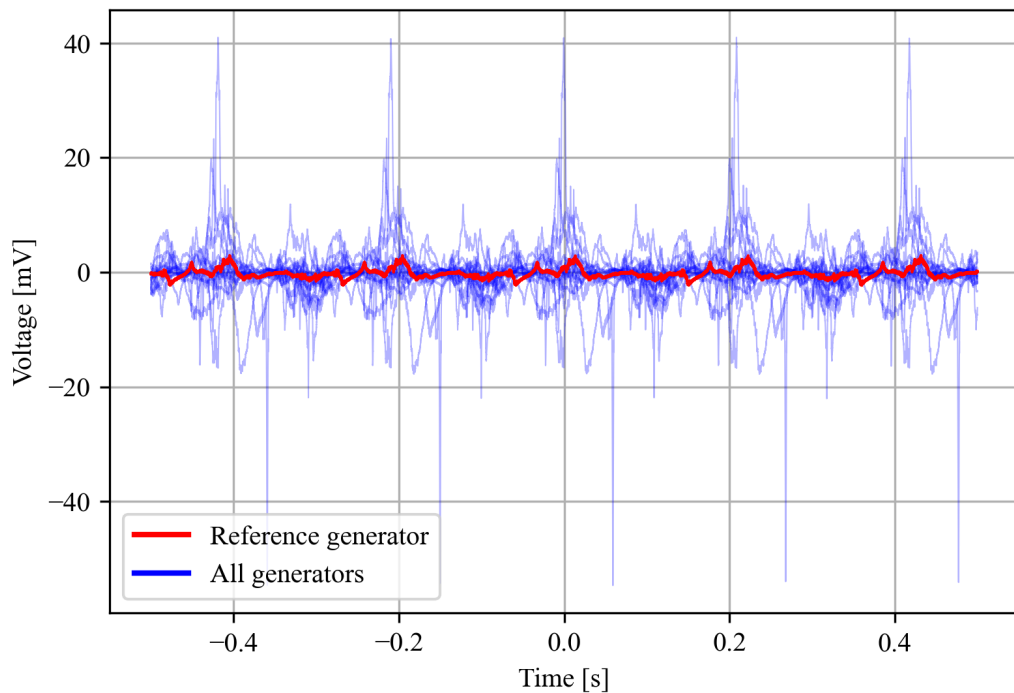

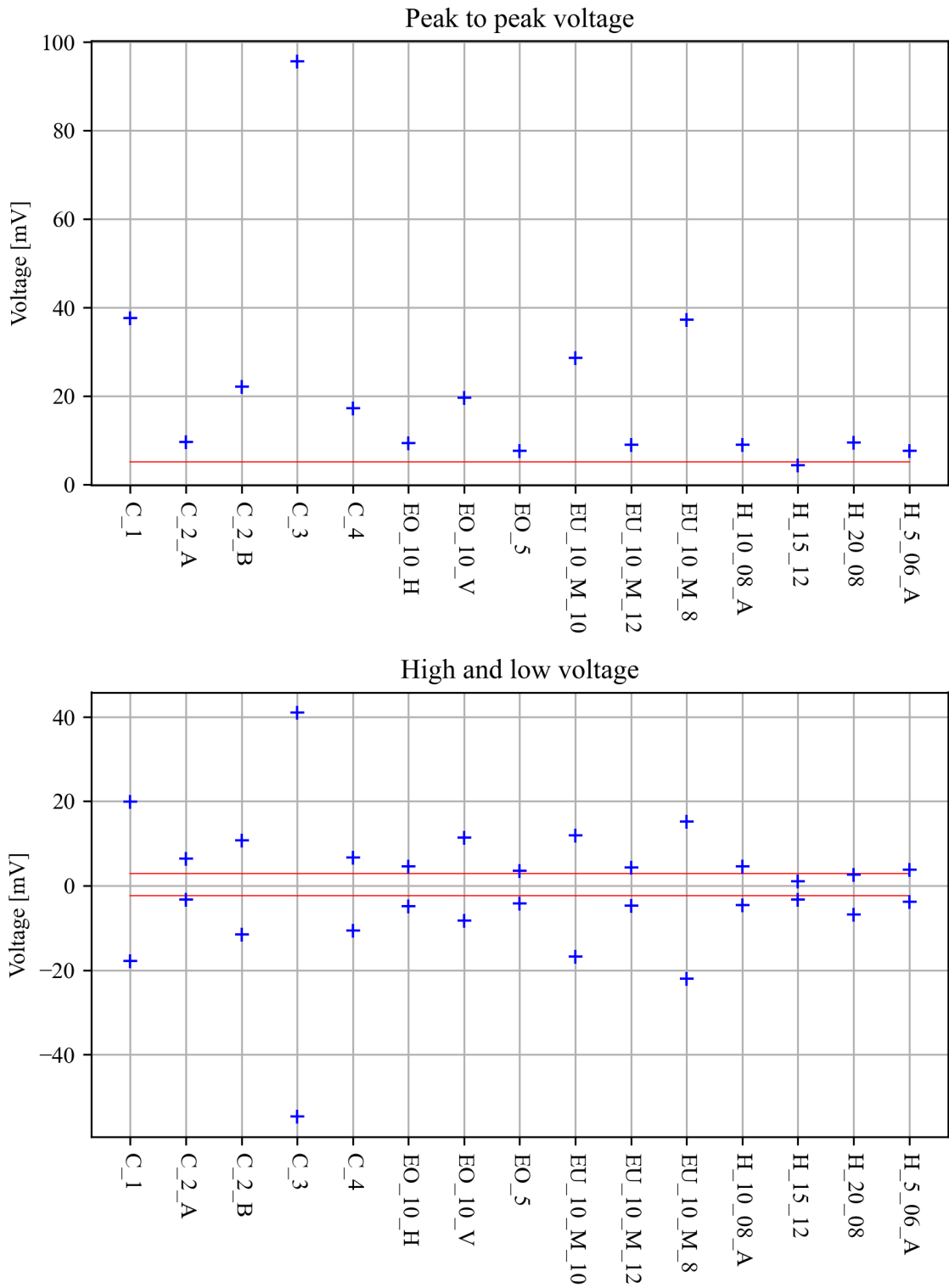Figure 3.17: Oscilloscope record of generated voltage for all generators (blue) and the reference generator (red)

Figure 3.18: P–P, high, and low generated voltage of all generators (blue) compared with the reference generator (red baseline)

3.5.4 Energy harvesting

The ability to charge a capacitor in an energy harvesting setup was tested for all manufactured generators. For all of them, it took too long to reach the maximum voltage to be captured using an oscilloscope. Therefore only the maximum voltage was monitored. Surprisingly all the manufactured generators performed the same including the reference generator maxing around 60 mV. This may be caused by external noise – harvesting energy from voltage generated by induction or another electro-mechanical phenomenon like a friction-generated electric charge.

If we compare these results with a commercially available PZT piezoelectric disc, the output of PVDF generators appears negligible since PZT elements easily charge the capacitor to several volts after just a few deformation cycles. But this comparison is not fair because we already know that PZT has piezoelectric constants several orders of magnitude higher than PVDF. But the purpose of this work is not to replace ceramics with polymers but rather to develop a polymer generator suitable for applications where ceramics cannot be used. Therefore it makes more sense to compare these results with another polymer piezoelectric element. Fortunately, just such a comparison was possible.

A piezoelectric energy generator based on electrospun PVDF film prepared by a Turkish research team was used for comparison. The manufacturing process of this generator is described in [29]. A photo of this generator is shown in Figure 3.19. This generator in the energy harvesting setup was able to charge the capacitor to around 200 mV.
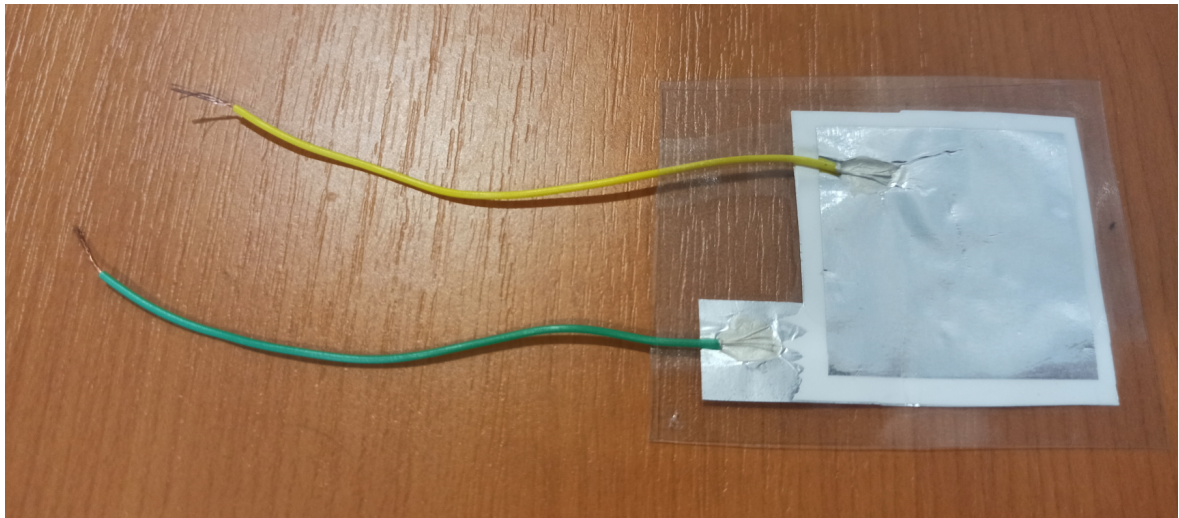
Figure 3.19: PVDF piezoelectric generator prepared by Turkish research team according to [29]

Let us discuss possible ways of improvement. Generators prepared within this work are based on PVDF layers. The PVDF powder used is a material primarily used for extrusion and injection molding of piping or packaging. It is sold in large volumes for a reasonable price. Therefore we were able to obtain a 1 kg sample free of charge. But it also means a lower chemical purity and no control over the material parameters like average molecular weight. For comparison, the typical source of PVDF in articles regarding this topic is Sigma Aldrich PVDF powder which costs around $1000 for 1 kg. This allows no room for scaling up the manufacture which we consider a key aspect of the research. Thus our choice of cheap high volume material.

Regarding the generator design performance definitely could be improved by ensuring better contact between the polymer layer and electrodes. In the current design, the outer GAG PET was too rigid and caused corrugation reducing the electrode-polymer contact area.

The measuring process could be improved as well. As demonstrated in [29] P–P voltage is strongly dependent on frequency therefore it would be very reasonable to measure this dependency for a whole suitable range of frequencies not only a single one.

Conclusion

Within this master's thesis, three methods for the preparation of PVDF films were successfully designed and performed. Using electrospinning layers of unoriented and oriented fibers deposited on aluminum foil and mylar were prepared. A method for fiber alignment was developed and applied to demonstrate the successful deposition of fibers aligned in one direction and in a rectangular grid proving the great potential of the electrospinning method. The casting method and water-assisted curing were used for self-supporting polymer films. Flexible piezoelectric generators based on these polymer layers were then manufactured and characterized by electromechanical methods. The highest observed peak-to-peak voltage was $U = 95.7$ mV. Samples prepared by water-assisted casting performed noticeably worse than samples prepared by other methods. No significant difference in performance was observed for samples prepared by electrospinning and casting. Therefore casting turned out to be a better method since it is simpler, cheaper, and easily scalable. Electrospinning on the other hand has great potential for use in other applications for example filtration. In an energy harvesting setup, all generators performed similarly. All managed to charge a capacitor to around 60 mV.

In conclusion, manufactured generators underperformed state-of-the-art PVDF generators prepared by similar methods but reasons and also possible ways for improvement were discussed. On the other hand, the electrospinning apparatus designed and constructed within this master's thesis together with the alignment analysis tool opens a whole new research stream for the Department of Experimental Physics with potential applications reaching far beyond piezoelectricity and energy harvesting.

Bibliography

[1] R. O. Ebewele, *Polymer Science And Technology.* CRC Press LLC, New York, 2000.

[2] S. Ramakrishna, K. Fujihara, W. E. Teo, T. C. Lim, and Z. Ma, *An Introduction to Electrospinning and Nanofibers.* World Scientific Publishing Co. Pte. Ltd., 2005.

[3] S. Ebnesajjad, "Introduction to plastics," in *Chemical Resistance of Engineering Thermoplastics* (E. Baur, K. Ruhrberg, and W. Woishnis, eds.), Plastics Design Library, pp. 13–25, William Andrew Publishing, 2016.

[4] F. Dickert and U. Latif, "Quartz crystal microbalances: Chemical applications," in *Comprehensive Supramolecular Chemistry II* (J. L. Atwood, ed.), pp. 201–211, Oxford: Elsevier, 2017.

[5] Graz University of Technology – online course – *Advanced Solid State Physics – Piezoelectricity* available at: https://lampx.tugraz.at/hadley/ss2/crystalphysics/-piezo.php.

[6] M. Vacula, "Characterization of piezoelectric materials and components." Bachelor's Thesis, Palacky University Olomouc, 2016.

[7] A. G. (https://electronics.stackexchange.com/users/117104/audio guy), "Maximum resonant impedance of a piezo disc." Electrical Engineering Stack Exchange. URL:https://electronics.stackexchange.com/q/246637 (version: 2016-07-18).

[8] D. Damjanovic, "Piezoelectricity," in *Encyclopedia of Condensed Matter Physics* (F. Bassani, G. L. Liedl, and P. Wyder, eds.), pp. 300–309, Oxford: Elsevier, 2005.

[9] Ceramic Manufacturing Series – Poling PZT Ceramics, APC Materials, Piezo Applications, 2016, available at: https://www.americanpiezo.com/blog/ceramic-manufacturing-series-poling-pzt-ceramics/.

[10] J. S. Harrison and Z. Ounaies, "Piezoelectric polymers," *ICASE NASA Langley Research Center Hampton*, Virginia, 2001.

[11] Y. Ting, H. Gunawan, A. Sugondo, and C. W. Chiu, "A new approach of polyvinylidene fluoride (PVDF) poling method for higher electric response," *Ferroelectrics*, vol. 446, pp. 28—-38, 2013.

[12] T. Wu, H. Jin, S. Dong, X. Peng, H. Xu, L. Lu, Z. Fang, S. Huang, X. Tao, L. Shi, and S. Liu, "A flexible film bulk acoustic resonator based on -phase polyvinylidene fluoride polymer," *Sensors*, vol. 20, p. 1346, 02 2020.

[13] V. Panna, S. Edina, D. András, H. Edit, G. Dorián, F. Balázs, D. Balázs, A. S. K., V. Tamás, V. Geert, M. György, and N. Z. K., "Scale-up of electrospinning technology: Applications in the pharmaceutical industry," *WIREs Nanomedicine and Nanobiotechnology*, vol. 12, no. 4, p. e1611, 2020.

[14] Z. He, F. Rault, M. Lewandowski, E. Mohsenzadeh, and F. Salaün, "Electrospun pvdf nanofibers for piezoelectric applications: A review of the influence of electrospinning parameters on the β phase and crystallinity enhancement," *Polymers*, vol. 13, no. 2, 2021.

[15] A. Sanyal and S. Sinha-Ray, "Ultrafine PVDF nanofibers for filtration of air-borne particulate matters: A comprehensive review," *Polymers*, vol. 13, p. 1864, 2021.

[16] Z. Q. Dong, X. hua Ma, Z. L. Xu, W. T. You, and F. bing Li, "Superhydrophobic PVDF—PTFE electrospun nanofibrous membranes for desalination by vacuum membrane distillation," *Desalination*, vol. 347, pp. 175—-183, 2014.

[17] P. M. Martinsa, S. Ribeiroa, C. Ribeiroab, V. Sencadasabc, A. C. Gomesd, F. M. Gamae, and S. Lanceros-Méndez, "Effect of poling state and morphology of piezoelectric poly(vinylidene fluoride) membranes for skeletal muscle tissue engineering," *The Royal Society of Chemistry*, vol. 3, pp. 17938–17944, 2013.

[18] I. Alghoraibi, *Different methods for nanofibers design and fabrication.* 02 2018.

[19] N. Sezer and M. Koç, "A comprehensive review on the state-of-the-art of piezoelectric energy harvesting," *Nano Energy*, vol. 80, pp. 1–25, 11 2020.

[20] S. Khalid, I. Raouf, A. Khan, N. Kim, and H. S. Kim, "A review of human-powered energy harvesting for smart electronics: Recent progress and challenges," *International Journal of Precision Engineering and Manufacturing-Green Technology*, vol. 6, 07 2019.

[21] S. Priya and D. J. Inman, *Energy Harvesting Technologies.* Springer Science+Business Media, LLC, 2009.

[22] M. Zeyrek Ongun, S. Oguzlar, U. Kartal, M. Yurddaskal, and O. Cihanbegendi, "Energy harvesting nanogenerators: Electrospun β-PVDF nanofibers accompanying zno nps and zno@ag nps," *Solid State Sciences*, vol. 122, p. 106772, 2021.

[23] M. Z. Ongun, L. Paralı, S. Oğuzlar, and J. Pechousek, "Characterization of β-PVDF-based nanogenerators along with fe2o3 NPs for piezoelectric energy harvesting," *J Mater Sci: Mater Electron*, vol. 31, pp. 19146—-19158, 2020.

[24] M. Zaccaria, D. Fabiani, A. Zucchelli, J. Belcari, and O. Bocchi, "Vibration energy harvesting using electrospun nanofibrous pvdf-trfe," vol. 2, pp. 796–799, 2016.

[25] A. Proto, B. Fida, I. Bernabucci, D. Bibbo, S. Conforto, M. Schmid, K. Vlach, V. Kasik, and M. Penhaker, "Wearable pvdf transducer for biomechanical energy harvesting and gait cycle detection," pp. 62–66, 2016.

[26] J. Yan, M. Liu, Y. G. Jeong, W. Kang, L. Li, Y. Zhao, N. Deng, B. Cheng, and G. Yang, "Performance enhancements in poly(vinylidene fluoride)-based piezoelectric nanogenerators for efficient energy harvesting," *Nano Energy*, vol. 56, pp. 662–692, 2019.

[27] Y. Zhang, M. Zhang, Y. Luo, and X. Zhang, "Energy harvesting characteristics of pvdf layers on thin-walled structures with curved surface," *Journal of Vibroengineering*, vol. 18, pp. 5029–5047, 12 2016.

[28] M. R. Mhetre and H. K. Abhyankar, "Human exhaled air energy harvesting with specific reference to pvdf film," *Engineering Science and Technology, an International Journal*, vol. 20, no. 1, pp. 332–339, 2017.

[29] M. Koç, L. Paralı, and O. Şan, "Fabrication and vibrational energy harvesting characterization of flexible piezoelectric nanogenerator (PEN) based on PVDF/PZT," *Polymer Testing*, vol. 90, p. 106695, 2020.

[30] V. Skoumal. Author's GitHub available at: https://github.com/VojtechSkoumal/-Masters-thesis.git.

[31] P. Bořil, "Pohybové zařízení mössbauerova spektrometru na bázilineárního magnetického motoru." Bachelor's Thesis, Palacky University, 2020.

[32] Y. Lin, E. Bilotti, C. W. Bastiaansen, and T. Peijs, "Transparent semi-crystalline polymeric materials and their nanocomposites: A review," *Polymer Engineering & Science*, vol. 60, no. 10, pp. 2351–2376, 2020.

[33] N. Yahya, S. Sikiru, A. Rostami, H. Soleimani, A. Shafie, B. Alqasem, S. Qureshi, and M. Ganeson, "Percolation threshold of multiwall carbon nanotube-pvdf composite for electromagnetic wave propagation," *Nano Express*, vol. 1, 06 2020.

List of symbols and shortcuts

A	area
A-PET	amorphous PET
BS	backscattered (electrons)
c	concentration $\%\ \frac{w}{V}\ \left(\frac{\text{PVDF weight}}{\text{solvents volume}}\right)$
C	capacity
δ	uncertainty
Δ	dwell time
d	needle-collector distance
DC	direct current
DMF	dimethylformamide
ϵ_{r}	relative permittivity
ϵ_0	permittivity of a vacuum
EDS	energy-dispersive X-ray spectroscopy
f	frequency
GAG PET	PET-G foil with A-PET core
HV	high voltage
LDPE	low density polyethylene
LED	light emitting diode
N	number of steps in full rotation
p	screw thread pitch
P–P	peak-to-peak (voltage)
PET	polyethylene terephthalate
PET-G	polyethylene terephthalate glycol-modified
PLA	polylactide
PP	polypropylene
PVDF	polyvinylidene difluoride
PZT	lead zirconate titanate
Q	flow rate
r	syringe radius
SEM	scanning electron microscope
τ	thickness
θ	phase angle
U	voltage
X_{c}	capacitance
Z	impedance